






This is to certify that the  
thesis entitled  
Laser Cladding of Hard-Facing Materials onto  
AISI 1045 Steel for Patterned Cutting-Die Design  
presented by

Yiping Hu

has been accepted towards fulfillment  
of the requirements for  
Master's degree in Materials Science

  
Major professor

Date 12/13/96

**LIBRARY**  
**Michigan State**  
**University**

**PLACE IN RETURN BOX** to remove this checkout from your record.  
**TO AVOID FINES** return on or before date due.

DATE DUE	DATE DUE	DATE DUE
<del>Aug 18 1977</del> _____	_____	_____
_____	_____	_____
_____	_____	_____
_____	_____	_____
_____	_____	_____
_____	_____	_____
_____	_____	_____

**LASER CLADDING OF HARD-FACING MATERIALS ONTO  
AISI 1045 STEEL FOR PATTERNED CUTTING-DIE DESIGN**

**By**

***Yiping Hu***

**A THESIS**

**Submitted to**

**Michigan State University**

**in partial fulfillment of the requirements**

**for the degree of**

**MASTER OF SCIENCE**

**Department of Materials Science and Mechanics**

**Michigan State University**

**East Lansing, MI 48824**

**1996**



## **ABSTRACT**

### **LASER CLADDING OF HARD-FACING MATERIALS ONTO AISI 1045 STEEL FOR PATTERNED CUTTING-DIE DESIGN**

**By**

***Yiping Hu***

In conventional rotary cutting-die manufacturing process, the cost of materials is high, the process is time-consuming, production efficiency is very low, and therefore production costs are extremely high. Also, the life of rotary cutting dies is rather short due to the segregation and flake morphology of carbides in D2 alloy, commonly used for die making. For this reason, it is necessary to seek a new tool material, with a hard surface, a tough core, and with wear-resistant properties, to form patterned cutting blades to prolong the life of rotary cutting dies. Alternatively, we can investigate an alternative manufacturing process to produce such cutting dies at a significantly reduced production cost. Laser cladding appears to be such a process.

In our present research, a new powder feeding system is designed for laser cladding. It can provide a stable, continuous, and accurate powder feeding rate, and deliver the powder stream coaxially into the molten pool under the laser beam. The experimental results showed that this powder feeding system is suitable for depositing high quality cladding tracks, along complicated geometric paths, on flat or curved

surfaces. A simple but realistic model relating the clad thickness and processing parameters is also developed, and the various relationships between the clad thickness and process parameters are discussed in detail. The calculated results of this model are in good agreement with the experimental ones. Finally, a novel process is successfully developed for directly depositing hard-facing tracks, along complicated geometric paths, on AISI 1045 steel substrates for manufacturing plate or rotary cutting dies. Fully functional prototype of industrial rotary cutting dies, for pilot testing, has been successfully produced by this process. This new technique is being implemented in die-making industry.

## **ACKNOWLEDGEMENTS**

I wish to thank my thesis advisor, Prof. K. Mukherjee, for his academic guidance, advice, and financial support throughout the duration of this work. I would also like to extend my sincere appreciation to Prof. P. Y. Kwon and Prof. K. N. Subramanian for their invaluable suggestions for improving this thesis.

Sincere gratitude is also extended to my wife and my parents for their encouragement, and spiritual support.

I would like to thank Dr. C. W. Chen, Dr. S. Kudapa, and J. Howard for their friendship and help. I would also like to thank Dr. Yu Zhang, in Bernal Division, Stevens Graphics Inc. for having the coaxial nozzle manufactured, and providing CPM 10V and CPM 15V alloy powders as well as AISI 1045 steel plates and rollers.

## TABLE OF CONTENTS

<b>LIST OF TABLES</b>	<b>viii</b>
<b>LIST OF FIGURES</b>	<b>ix</b>
<b>1 INTRODUCTION</b>	<b>1</b>
1.1 Background and Motivation.....	1
1.2 Scope.....	4
<b>2 REVIEW OF LASER SURFACE TREATMENT PRINCIPLE</b>	<b>6</b>
2.1 Principle of Laser Operation.....	6
2.1.1 The Nd:YAG laser.....	7
2.1.2 The CO <sub>2</sub> laser.....	8
2.2 Laser-Beam Mode.....	9
2.3 Laser Parameters.....	11
2.3.1 Laser-Beam Diameter.....	11
2.3.2 Laser-Beam Power.....	11
2.3.3 Power Density.....	12
2.4 Laser Beam-Material Interaction.....	12
<b>3 LASER SURFACE TREATMENT</b>	<b>15</b>
3.1 Laser Solid-Transformation Hardening.....	15
3.2 Laser Remelting.....	16
3.3 Laser Alloying.....	16
3.4 Laser Dispersing.....	17
3.5 Laser Cladding.....	18
3.5.1 General Description.....	18
3.5.2 Scope of Laser Cladding.....	18
3.5.3 Processing Parameters.....	19

3.5.3.1	Absorptivity. ....	19
3.5.3.2	Traverse Speed. ....	20
3.5.3.3	Powder Feeding Techniques. ....	21
3.5.3.4	Shielding Gas. ....	22
3.5.4	Advantages of Laser Cladding Process. ....	22
3.5.5	Limitations of Laser Cladding Process. ....	23
3.5.6	Applications of Laser Cladding Process. ....	23
<b>4</b>	<b>EXPERIMENTAL PROCEDURES</b>	<b>25</b>
4.1	General Description. ....	25
4.2	Choice of materials. ....	26
4.2.1	Substrate Materials. ....	26
4.2.2	Clad Materials. ....	27
4.3	Laser Cladding System. ....	30
4.3.1	Laser Generator. ....	30
4.3.2	Beam Delivery System. ....	30
4.3.3	Powder Feeding System. ....	32
4.3.3.1	Powder Feeder. ....	34
4.3.3.2	Powder-Flow Splitter. ....	34
4.3.3.3	Coaxial Nozzle. ....	36
4.3.4	CAM System. ....	38
4.4	Laser cladding. ....	38
4.5	Post-Clad Treatment. ....	43
4.6	Microstructures and Hardness Measurements. ....	43
<b>5</b>	<b>RESULTS AND DISCUSSION</b>	<b>44</b>
5.1	Measurement of Powder Utilization Coefficient. ....	44
5.2	Relationships between Clad Width and Process Parameters. ....	51
5.3	Process Modeling. ....	57
5.3.1	Assumptions. ....	57
5.3.2	Basic Equation. ....	57
5.3.3	Energy-Density Equation. ....	59

5.3.4	Clad Thickness-Energy Density Equation, . . . . .	60
5.4	Correlation Derived from Basic Equation, . . . . .	61
5.4.1	Relationship between Clad Thickness and Traverse Speed, . . . . .	61
5.4.2	Relationship between Clad Thickness and Spot Size, . . . . .	61
5.4.3	Relationship between Clad Thickness and Powder Feed Rate, . . . . .	62
5.5	Correlation Derived from the Energy-Density Equation, . . . . .	66
5.5.1	Relationship between Energy density and Spot Size, . . . . .	66
5.5.2	Relationship between Energy density and Traverse Speed, . . . . .	66
5.5.3	Relationship between Energy density and Laser Power, . . . . .	67
5.6	Correlation between Clad Thickness and Energy Density, . . . . .	71
5.7	Comparisons of Calculated and Experimental Results, . . . . .	72
5.7.1	Clad Thickness and Traverse Speed, . . . . .	72
5.7.2	Clad Thickness and Spot Size, . . . . .	75
5.7.3	Clad Thickness and Powder Feed Rate, . . . . .	77
5.7.4	Clad Thickness and Energy Density, . . . . .	79
5.8	Correlation between Penetration Depth and Energy Density, . . . . .	81
5.9	Microstructure, . . . . .	83
5.9.1	Geometric Characteristics of A Single Cladding Track, . . . . .	83
5.9.2	Vanadium Carbides, . . . . .	92
5.10	Microhardness of A Single Clad Track, . . . . .	93
5.11	Manufacturing of Patterned Rotary Cutting Die, . . . . .	96
<b>6</b>	<b>CONCLUSIONS</b>	<b>103</b>
	<b>BIBLIOGRAPHY</b>	<b>106</b>

## LIST OF TABLES

1	Chemical compositions of substrate and clad materials. ....	27
2	Characteristics of the RF exited CO <sub>2</sub> laser. ....	30
3	CNC machine specifications. ....	38
4	Measurements of powder utilization coefficient $\alpha$ . ....	46
5	Correlation between clad width and processing parameters. ....	52
6	Processing parameters used to develop the correlation between clad thickness and reciprocal of traverse speed. . . . .	73
7	Processing parameters used to develop the correlation between clad thickness and reciprocal of spot size. ....	76
8	Processing parameters used to develop the correlation between clad thickness and powder feed rate. ....	78
9	Processing parameters used to develop the correlation between clad thickness and energy density. ....	80
10	Processing parameters used to develop the correlation between penetration depth and energy density. ....	81
11	Processing parameters for producing rotary cutting dies. ....	97

## LIST OF FIGURES

1	Transverse mode patterns in cylindrical and rectangular coordinates [5]. . . . .	10
2	Wear resistance of CPM 10V and conventional tool steels at indicated hardness [80]. CPM 10V* (hardened) is subjected to quenching, which increases its hardness, and thus the extra wear resistance. . . . .	28
3	Charpy C-notch impact properties of CPM 10V and conventional tool steels at indicated hardness [80]. . . . .	29
4	A schematic of laser cladding system. . . . .	31
5	A view of side powder feeding system. . . . .	33
6	A view of cone-shaped powder stream. . . . .	35
7	A schematic of transverse section of a coaxial nozzle. . . . .	36
8	A view of single cladding tracks with smooth surface on a steel plate. . . . .	41
9	A view of intersecting hard-facing cladding tracks directly deposited on a steel roller. . . . .	42
10	Plot of powder utilization coefficient vs. traverse speed. . . . .	49
11	Plot of powder utilization coefficient vs. powder feed rate. . . . .	49
12	Plot of powder utilization coefficient vs. laser spot size. . . . .	50
13	Clad width as a function of traverse speed. . . . .	55
14	Clad width as a function of energy density. . . . .	55
15	Clad width as a function of powder feed rate. . . . .	56
16	Parabolic shape of the cross-section of a clad track. . . . .	58
17	Clad thickness as a function of reciprocal of traverse speed. . . . .	63
18	Clad thickness as a function of reciprocal of spot size. . . . .	64
19	Clad thickness as a function of powder feed rate. . . . .	65
20	Energy density as a function of reciprocal of spot size. . . . .	68



21	Energy density as a function of reciprocal of traverse speed. ....	69
22	Energy density as a function of laser power. ....	70
23	Clad thickness as a function of energy density. ....	71
24	Comparison of calculated and experimental relationship between clad thickness and reciprocal of traverse speed. (a) $v < 8.4$ mm/sec. (b) $v \geq 8.4$ mm/sec. ....	74
25	Comparison of calculated and experimental relationship between clad thickness and reciprocal of spot size. ....	77
26	Comparison of calculated and experimental relationship between clad thickness and powder feed rate. ....	79
27	Comparison of calculated and experimental relationship between clad thickness and energy density. ....	80
28	Penetration depth as a function of energy density. ....	82
29	Three basic single clad bead profiles. (a) Deep penetration clad bead. (b) Clad bead with a reasonable width to height aspect ratio. (c) Parabolic clad bead. ....	85
30	Optical micrographs of cross section of clad tracks with no macroscopic cladding defects. (a) $v = 3$ mm/sec. (b) $v = 3.9$ mm/sec. (c) $v = 4.9$ mm/sec. (d) $v = 5.8$ mm/sec. (e) $v = 6.6$ mm/sec. Other processing parameters are as follows: P = 2073 watts, D = 1.8mm, and $F_p = 0.167$ gm/sec. ....	86
31	Effect of laser power on clad formation. (a) P = 2073 watts. (b) P = 1755 watts. (c) P = 1567 watts. (d) P = 1110 watts. Other processing parameters: $v = 8.4$ mm/sec, D = 2.3 mm, and $F_p = 0.167$ gm/sec. ....	89
32	A magnified optical micrograph of figure 31 (d), showing the lack of fusion between the clad and substrate. ....	91
33	A view of carbides in CPM 10V and D2 alloys. (a) Fine vanadium carbide particles uniformly dispersed in the matrix in CPM 10V clad. (b) Segregation and flake morphology of carbides in D2 alloy. ....	93
34	Microhardness profiles of the cladding track. (a) As-clad. (b) As-clad + tempering. (c) As-clad + tempering + liquid nitrogen treatment. ....	96
35	A view of intersecting hard-facing tracks, with smooth surfaces, uniform clad thickness, and width, deposited on a AISI 1045 steel flat plate. ....	99

36	A view of the hard-facing tracks, directly deposited onto a AISI 1045 steel roller by laser cladding process. ....	100
37	Hard-facing tracks, with complicated geometric patterns, deposited on a AISI 1045 steel roller via laser cladding. ....	101
38	A view of hard-facing tracks, with complex geometric patterns, deposited on a steel roller by laser cladding after surface grinding. ....	102

# **Chapter 1**

## **INTRODUCTION**

### **1.1 Background and Motivation**

In packaging industry, rotary cutting dies have been widely used to cut cereal and soft beverage boxes, facial paper towels, paper money, credit cards, and disk floppies, and so on. The cutting speed is so fast, and impact loads and shear stresses are so large that the service life of rotary cutting dies is very short. Typically, such rotary cutting dies can work for one or two months depending on the chemical compositions, hardness, and other properties of the materials to be cut.

In conventional rotary cutting-die manufacturing process, the die-block and the cutting blades are made of an expensive tool steel D2. In order to prevent the distortion of the cutting blades, the entire die-block is first hardened to obtain the hardness of HRC 60, then the hardened block is machined by electrical discharge machining (EDM) to produce the cutting blades. Thus, for the conventional process, the cost of materials is high, the process is time-consuming, the production efficiency is very low, and therefore the overall production costs are extremely high. As mentioned before, the working environment of rotary cutting dies is very severe. Because of pronounced ingot segregation, conventional tool steels often contain a coarse, nonuniform microstructure accompanied by poor transverse properties. Therefore, the life of the rotary cutting dies

made of D2 alloy is rather short due to the segregation and flake morphology of carbides in D2 alloy.

In order to greatly improve the life of the cutting dies, a new wear-resistant tool material with hard surface and tough core, or a new process has to be sought to form the patterned cutting blades, which can withstand imposed service loads without deformation, fracture, and excessive wear. In terms of practical application of the rotary cutting dies, only the cutting blades are used for cutting functions. Therefore the die block made entirely of an expensive tool steel D2 is completely wasteful. It is necessary to investigate a novel processing technique to produce such cutting dies at a significantly reduced production cost.

Laser surface cladding offers the potential to deposit new materials with special properties onto different substrates. By this process, high wear-resistant, corrosion-resistant, and oxidation-resistant coatings, in the shape of cutting blades, can be deposited on selected areas and/or in a precisely defined pattern on a variety of substrates. For example, metal carbides, or metal/carbide mixtures can be injected to laser-generated molten pool, on a substrate, to form a composite layer on the surface to improve wear property of tool steel, and prolong the surface life of forging dies [1-2]. However, the base materials are still very expensive. To date, no published literature describes any technology for manufacturing plate and rotary cutting dies by laser cladding process. It is this observation that led us to investigate the feasibility of developing such a new technique.

From our laser material processing experience, we realized the potential application of the laser cladding process in manufacturing cutting dies. Through our

arduous efforts, and repeated analysis of experimental variables, we have succeeded in developing a novel technology for manufacturing plate and rotary cutting dies. Fully functional prototype of industrial cutting dies, for pilot testing, has been successfully produced by this process. Also, this new technology has greater manufacturing flexibility because different substrates and reinforcement materials, with required mechanical properties, can be chosen to adapt to the different applications.

Compared with the conventional cutting-die manufacturing processes, this technology, in which cutting blades, with complicated geometric patterns, are directly deposited by laser cladding onto a substrate, has many advantages:

- Material cost can be greatly reduced because an expensive tool steel body of the die-block can be replaced by a cost-effective structural steel.
- Production costs can also be significantly reduced due to the elimination of costly heat treatment, and the reduced demand on the EDM.
- Durability of the cutting die is expected to be significantly improved because the wear resistant property of hard-facing material is much better than that of the tool steel D2, currently used in industry.
- Production efficiency could be much higher than that of the conventional process due to the reduced demand on the EDM, and the elimination of the costly tool steel heat treatment.
- Such a processing technique can also be used for repairing the worn cutting blades.
- The new processing technology could be more flexible because different substrates and clad materials, with desired mechanical properties, could be chosen for various applications.

## 1.2 Scope

The aims of this research are to develop a processing parametric model based on the physical phenomena and geometric features of single cladding tracks in laser cladding process, and to investigate the feasibility of developing a novel process technique for manufacturing plate and rotary cutting dies by laser cladding process. The detailed requirements are as follows:

- Design a new powder feeding system to provide a stable, continuous, and accurate powder feeding rate, and deliver the powder stream coaxially into the molten pool on the surface of a substrate under the laser beam.
- Perform preliminary experiments to obtain initial processing parameters, such as laser power, spot size, traverse speed, powder feed rate, and shielding gas flow rate.
- Develop a simple but realistic model, relating the maximum clad thickness and processing parameters, discuss in detail the various relationships between the clad thickness and different processing variables, and determine the minimum energy density for clad formation under the experimental condition.
- Characterize the microstructures of cladding layer, interface, and heat-affected zone by using optical microscopy, and measure the microhardness of cross section of the samples under the following conditions: 1) as-clad, 2) as-clad + tempering, and 3) as-clad + tempering + liquid nitrogen treatment.
- Eliminate any unacceptable defects in the clads, such as porosity, microcracks, and poor metallurgical bonding between the clad and substrate by modifying the process parameters and other related factors.

- Based on the basic study, investigate the feasibility of depositing a high wear-resistant alloy powder, CPM 15V, on AISI 1045 medium carbon steel for making plate or rotary cutting dies, with complicated geometric patterned cutting blades, by laser cladding process.

## **Chapter 2**

### **REVIEW OF LASER SURFACE TREATMENT PRINCIPLE**

#### **2.1 Principle of Laser Operation**

The laser, which is an acronym for light amplification by stimulated emission of radiation, is a source of optical frequency radiation which is coherent, controllable, and intense. It is these properties that make such lasers as Nd:YAG and CO<sub>2</sub> competing heat sources to be widely used for materials surface modifications.

Every laser is composed of three main components: amplifying medium or active medium, means of excitation, and an optical resonator [3-4]. The amplifying medium determines the laser wavelength and the type of excitation required. A medium is potentially used as an optical frequency amplifier if the population of its energy levels can be altered so that there are more emissions than absorptions per unit time. That is so called the population inversion, which is absolutely necessary for amplification of light to occur. Otherwise, a beam of light directed through the active medium with photon energy will be absorbed.

In terms of the different energy state schemes, population inversion requires excitation of atoms or molecules to the higher laser level by pumping methods or means of excitation. Pumping methods includes optical pumping, gas discharge pumping, and chemical reaction pumping. The use of pumping methods really depends on the active medium. For Nd:YAG and CO<sub>2</sub> lasers, optical pumping and gas discharge pumping are



employed, respectively, to create excited atoms or the passages of an electrical discharge through gaseous media to produce collisionally excited atoms or molecules. The former is used to excite an Nd:YAG crystal to lase at  $1.06\text{ }\mu\text{m}$ , and the latter is used to excite a  $\text{CO}_2$  gas laser at  $10.6\text{ }\mu\text{m}$ .

The optical resonator consists of a system of mirrors. Such a device causes the light emitted parallel to its axis to reflect back and forth through the amplifier. When the amplifier gain is equal to the round trip losses in the resonator the combination of the amplifier and resonator is at the threshold for lasing. Upon reaching or exceeding threshold the light in the resonator traveling parallel to its axis is amplified many times. The fraction removed on each pass by transmission through the output coupler results in a laser beam. Such multiple use of the amplifier leads to highly energetic laser outputs.

### **2.1.1 The Nd:YAG Laser**

The Nd:YAG laser is by far the most commonly used type of solid-state laser. Neodymium-doped yttrium aluminum garnet (Nd: YAG) possesses a combination of properties uniquely favorable for laser operation. The YAG host is hard, of good optical quality, and has a high thermal conductivity. Furthermore, the cubic structure of YAG favors narrow fluorescent linewidth, which results in high gain and low threshold for laser operation. In Nd:YAG, about 1% trivalent yttrium is substituted by trivalent neodymium, so charge compensation is not required. While  $\text{Nd}^{3+}$  ion exhibits a satisfactorily long fluorescence lifetime and narrow fluorescence linewidths, and possesses a terminal state for the laser transition sufficiently high above the ground state so that continuous-wave operation at room temperature is readily feasible. Therefore, this ion is usually incorporated as a dopant, called lasing medium. Due to special properties of

trivalent neodymium, a higher power level has been obtained from Nd lasers than from any other four-level material [5-7].

When excited by light from an electric discharge lamp  $\text{Nd}^{3+}$  ions in the YAG host in a proper optical resonator can cause the stimulated emission at a number of frequencies within three different groups of transitions centered at 0.9, 1.06, and 1.35  $\mu\text{m}$ . The most efficient laser operation is obtained when the optical resonator is designed for 1.06  $\mu\text{m}$ . This is the wavelength used in Nd:YAG lasers for materials interactions.

Recently, Nd:YAG lasers become of interest for materials surface treatments because multi-kilowatt systems now are on the market. The maximum power for Nd:YAG sources that can be purchased is about 2.5 kW in continuous-wave mode or about 3 kW average power in a pulsed laser system.

### **2.1.2 The $\text{CO}_2$ Laser**

In carbon dioxide lasers, carbon dioxide, nitrogen, and helium gases are mixed in the laser tube. The gas tube is placed in an optical resonator. When the gas discharge is induced by applying the electric field to the gas tube, the electronic bombardment and the ionic collision with helium ions excite the nitrogen molecules to their vibrational quantum states. When the excited nitrogen molecules collide with ground state  $\text{CO}_2$  molecules, the nitrogen molecules lose their energy and return to the ground state. The  $\text{CO}_2$  molecules in the ground state are excited to the higher energy state by this bombardment. The excited  $\text{CO}_2$  molecules take downward transitions to the lower energy state, producing the emission of radiation at 10.6  $\mu\text{m}$  wavelength. Because of the relaxation effect of helium, carbon dioxide molecules in the lower energy level eventually return to their ground states. This process cools the  $\text{CO}_2$  gas and reduces losses due to

absorption of 10.6  $\mu\text{m}$  light by lower to upper laser level transitions. Since the useful transitions in a carbon dioxide laser are based on vibrational molecular quantum states, the transition energies are low. Therefore, it operates in the infrared wavelength [4, 5, 8].

Although the transition energies are low, the transition energy per unit time is large or the operational power is high. Today high power continuous-wave  $\text{CO}_2$  lasers are commercially available with output power up to 25 kW.

## 2.2 Laser-Beam Mode

The spatial distribution of the electromagnetic field inside the optical cavity of a laser is described by resonant electromagnetic modes, which is referred to as the configurations of electromagnetic field inside a laser resonator cavity. By convention, the modes are indexed as  $\text{TEM}_{mn}$ , meaning transverse electromagnetic mode with  $m$  number of radial zero fields and  $n$  number of angular zero fields. The Figure 1 illustrates some  $\text{TEM}_{mn}$  modes in cylindrical and rectangular coordinates [4]. Beam divergence, beam diameter, and intensity distribution along the plane of the laser beam's cross section are governed by the transverse modes. The lowest order mode is  $\text{TEM}_{00}$ , which has a Gaussian-like intensity distribution. The laser beam in  $\text{TEM}_{00}$  can be focused to the smallest spot diameter on a workpiece surface in order to achieve the highest power density. A laser beam with  $\text{TEM}_{01}$  has a ring of intense energy surrounding a circle with no intensity, and this mode is commonly referred to as a "donut" mode. For laser surface treatment processes, low-order laser beams are usually used due to more uniform intensity distribution.

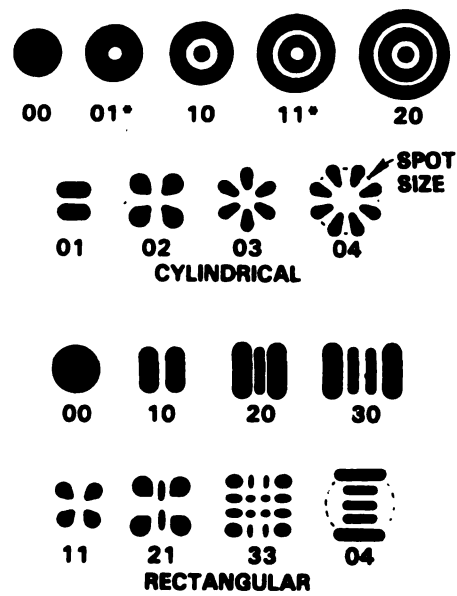


Figure 1- Transverse mode patterns in cylindrical and rectangular coordinates [4].

## 2.3 Laser Parameters

### 2.3.1 Laser-Beam Diameter

Laser-beam diameter is one of the two important variables determining the power density for a given incident laser-beam power. Because of the nature of the laser beam and the definition of the beam diameter, it is very difficult to measure the beam diameter for high-power laser beams. One definition has been established that the Gaussian beam diameter can be defined as the diameter where the laser power has dropped to  $1/e^2$  or  $1/e$  of the central value. The beam diameter defined on the basis of  $1/e^2$  of the central value contains almost 86% of the total power, whereas the diameter defined on the basis of  $1/e$  of the central value contains slightly over 60% of the total power. Therefore, the  $1/e^2$  beam diameter is usually adopted [9].

Because the spatial distribution of energy in the laser beam affects the focusing characteristics of the beam, the laser beam can not be focused to one point on a workpiece surface. For a Gaussian beam, the diffraction limited focal spot size,  $d_{\min}$ , is expressed by the relationship:  $d_{\min} = 1.27f\lambda / D$ , where "f" is the focal length of the focusing optics, and " $\lambda$ " is the wavelength of the laser beam, and "D" is unfocused beam diameter. The actual value will be larger due to aberrations and other imperfections of the focusing optic system.

### 2.3.2 Laser-Beam Power

Laser-beam power is one of the main processing variables for laser surface treatment. Incident laser power and laser-beam diameter determine the power density in the interaction zone, and laser power and traverse speed determine the treatable clad volume per unit time for a given powder feeding rate.

### 2.3.3 Power Density

Power density is defined as the incident laser-beam power per unit area. According to this definition, power density can be expressed by the relationship:  $P_d = P/A$ , where  $P_d$  is the power density,  $P$  is the incident laser-beam power, and  $A$  is the irradiation area. The power density is a main parameter for laser surface treatment since it determines the process functions, efficiency, and quality.

For power density values up to about  $10^4 \text{ W/cm}^2$ , the absorbed energy depends on the wavelength  $\lambda$ , the material, and the surface conditions of the interaction zone. The situation would be typical for solid transformation hardening.

When power density values increase to the order of  $10^5 \text{ W/cm}^2$ , the material in the interaction zone begins to melt in a hollow seam. This case would correspond to the processes of conduction welding, surface melting, alloying, and cladding.

The powder density values in the order of  $10^6 \text{ W/cm}^2$  leads to the formation of a vapor hole which is approximately focused laser spot size ("keyhole") surrounded by molten material. This situation will correspond to the processes of drilling and deep penetration welding.

## 2.4 Laser Beam-Material Interaction

In metals the incident laser radiation is predominantly absorbed by free electrons in the conduction band. The photon of the incident laser radiation has relatively low energy. For example, the energy of  $\text{CO}_2$  laser photons is only 0.12 eV while the photons obtained from the Nd:YAG laser have about 1.2 eV of energy. When a laser beam strikes a metal surface, heat transfer occurs by photon/electron interactions with free or bound electrons. These interactions raise the energy state of the electrons in the conduction

band. The excited electrons collide with other photons and electrons, and give back their radiation by spontaneous emission. In this way, the electronic energy derived from the photons of the incident laser radiation is converted into the heat energy. It is this heat energy that is used for laser surface treatments. In practice, most metals behave in this manner for light wavelengths exceeding about  $0.5\text{ }\mu\text{m}$ , which includes both YAG and  $\text{CO}_2$  lasers. Previous studies have shown that most of this absorption occurs in the shadow surface layer of metals, typically a few atomic layers, so that laser absorption in metals is truly a surface effect.

The interaction of high-power laser radiation with metals is capable of providing a novel and useful processing tool. However, it is difficult to obtain effective energy coupling between the incident laser radiation and workpiece due to the high reflection of metals. At room temperature, most pure metals and alloys absorb the less of the incident laser radiation, about one percent for copper and tens of percent for steels, for example, so that most of incident laser power is reflected from the metal surface. In order to yield an effective process, it is necessary to obtain the adequate laser energy at the workpiece, and couple a fraction of the incident laser energy as high as possible into the materials.

The efficiency with which a material absorbs the incident laser radiation is defined as the material's absorbance. It has been found that the absorbance of a surface is a function of the materials, nature of the surface, the level of oxidation, temperature, and wavelength and power density of the incident laser radiation [9]. Therefore, improving the nature of a metal surface or use of lasers with shorter wavelengths can greatly enhance its absorption. For a  $\text{CO}_2$  laser beam with  $10.6\text{ }\mu\text{m}$  wavelength at normal incidence, the absorptivity of most metals is less than 10%, while for a Nd:YAG laser beam with  $1.06$

$\mu\text{m}$  wavelength at the same incident angle, the absorptivity varies from 3.6 to 43%. In addition, increase in the roughness of a metal surface also can enhance the absorptivity by a factor of 1.2 to 1.5.

Although metals severely reflect  $\text{CO}_2$  laser beams, up to now, the lasers used for material surface modifications mainly are  $\text{CO}_2$  lasers due to their high available power level. In order to improve the absorptivity of metals at  $10.6 \mu\text{m}$  wavelength of  $\text{CO}_2$  laser beams, surface coatings, such as colloidal graphite coating and paint coating, and surface oxidation by chemical or heat treatment processes [10-11] are widely used in industry. By this process, the absorptivity can be increased to values of 70 to 80%.



## **Chapter 3**

### **LASER SURFACE TREATMENT**

The use of high-power laser beams has opened a novel category of processing opportunities in metal surface treatment and composite material fabrication. Laser materials processing is characterized by concentrating an extremely high power density on a small area of the alloy surface to achieve very rapid heating and cooling of the near surface of materials. During laser irradiation, with or without alloy powder injection, the substrate surface can be modified by changing either its alloy composition and structure, or only its structure. Because laser surface treatment (LST) belongs to a kind of rapid melting and solidifying process [12], it can extend solid solution, form metastable phases, refine the grain size, and hence improve the wear resistant, corrosion resistant, and oxidation properties of the treated materials.

Depending upon the main processing variables, power density, and interaction time, different laser surface treatment processes, such as laser hardening, remelting, surface alloying, dispersing, and cladding, have been developed. The definition and function of laser surface modifications are succinctly described as follows:

#### **3.1 Laser Solid-Transformation Hardening**

The laser surface hardening is usually used to harden the selected surface region of iron-base alloys. Laser-induced transformation hardening is based on the principle: the surface layers of an alloy is heated locally to transform to austenite and is then rapidly

quenched by conducting heat to the bulk material. This leads to the formation of a hard martensitic layer. By this process, laser heat treatment can improve the wear resistance of the treated material [13-17], Because a certain volume fraction of the martensitic phase transformation at the surface layers of a substrate is contributed to an increase of hardness in these surface regions.

### **3.2 Laser Remelting**

Laser remelting can improve the wear resistance and corrosion resistance of the thin surface layers of different alloys by homogenizing and refining the surface microstructure through rapid self-quenching. Through this process, high cooling and solidification rates can lead to the formation of fine and homogeneous microstructures. For this reason, the properties of the treated surface layers can be improved. Taking tool steels for example, due to the high solidification rates, carbon diffusion is suppressed, and the high temperature phases with their increased solubility limits are quenched down to room temperature. The resulting fine and homogeneous microstructure of the remelted tool steel leads to the improvement of wear and corrosion resistance. The metallic materials suitable for laser remelting process include cast iron [18-22], aluminum alloys [23-24], low and medium carbon steels [25-26], and tool steels [27-28].

### **3.3 Laser Surface Alloying**

Unlike laser remelting, laser surface alloying is usually used to change the chemical composition and microstructures of the surface layers of a substrate by simultaneous surface melting and injection of alloying elements, and hence creates a new surface alloy with the novel structures and required properties, such as wear resistance, corrosion resistance, and high-temperature oxidation resistance. The chemical

composition of the formed surface alloy not only depends on the composition of the materials involved, but also on the degree of mixture. In other words, the base material and the added materials must be adapted to achieve the required structures and properties. By laser alloying process, the high temperature in the melt pool can dissolve the stable phases like intermetallic compounds, the convection in the melt pool causes a good intermixing of the molten substrate with the alloying elements added, and the rapid solidification leads to the formation of fine and homogeneous structures. Laser surface alloying with alloying elements, such as C, Ni, Cr, Mo, W, Co, Mn, and Ti, is usually used to improve the wear resistance and corrosion resistance of different kinds of steels [29-37], aluminum alloys [38-39] and titanium alloys [40-41].

### **3.4 Laser Dispersing**

Laser dispersing is a special type of alloying process. During this process, the carbide particles with a high melting point are injected into the melt pool so that composite layers form after rapid solidification. The formed composite layers mainly consist of injected hard particles uniformly dispersed in the metallic matrix with a lower melting point. In order to obtain a good wear behavior of the layers produced by laser dispersing, a low dissolution of the injected hard particles is necessary. For laser dispersing, metal carbides, such as WC, TiC, VC, Mo<sub>2</sub>C and SiC, are usually used as hard particles. A significant number of publications report that this process has been developed to inject hard carbide particles into different metal substrates, such as steels [42-47], aluminum alloys [48-49], and titanium alloys [50-52], and wear resistance of the surface layers has been significantly improved. Because high percentage of carbides may lead to

the reduction in ductility of the composite layers, the dispersing process possibly causes cracking [53].

### **3.5 Laser Surface Cladding**

#### **3.5.1 General Description**

Laser surface cladding is a process in which an alloy powder or metal/carbide mixtures are allowed to interact with the laser beam on the surface of the substrate to form a rapidly solidified cladding layer with the required properties, such as high hardness, high wear resistance, high corrosion resistance, and high-temperature oxidation resistance, without affecting the performance of the bulk material. Unlike laser alloying, the chemical composition of the clad layer is usually very close to that of the alloy powder used because the dilution of the cladding layer can be controlled by choosing optimized process variables. Generally, a good clad has characteristics of uniform coating thickness and smooth surface, porosity- and cracks-free, minimum dilution and distortion, and good metallurgical bonding with the substrate.

#### **3.5.2 Scope of Laser Cladding**

For laser cladding process, different kinds of ferrous and non-ferrous alloys are usually used as the substrates, and the clad materials used really depend on the application purposes. For example, laser cladding with reinforcement materials, such as Fe-Cr-C-W, Co-Cr-C-W, Ni-Cr-B-Si or Fe-Cr-Ni, is widely used to improve the wear and corrosion resistance of plain and mild carbon steels [54-59], laser cladding with nickel base alloys is used to improve the wear resistance of aluminum alloys [60-61], and laser cladding with Ni-Cr-Al-Hf improves the high temperature oxidation resistance of nickel-base superalloys [62-63].

Laser cladding by carbide/metal composite powder on steels, aluminum, nickel, and titanium base alloys has shown its application potential for becoming a widely used hard-facing technique. Optimized combinations of basic material, metallic binder, and hard material allow the composite layers to be produced. The composite powder is usually made up of hard particles, such as SiC, WC, TiC, and VC, and ductile cobalt or nickel base alloys, and the produced cladding layers display high wear-resistant and corrosion-resistant properties [64-69].

### **3.5.3 Processing Parameters**

Both applications and efficiency of laser surface treatments strongly depend on process variables. The main process parameters for laser cladding include incident laser-beam power, laser-beam spot size and shape, laser absorptivity of the substrate, traverse speed, powder feed rate, and shielding gas flow rate. Laser parameters are discussed in Chapter 2, and the remaining processing parameters are described as follows:

#### **3.5.3.1 Absorptivity**

As has been stated before, for an optically opaque material, the absorptivity is referred to as the fraction of the laser energy absorbed by the substrate material. It has been found that, because the infrared absorption of metals mainly depends on the conductive absorption by free electrons, the absorptivity is a function of the electrical resistivity of the substrate [11]. The smaller the electrical resistivity, the lower is the absorptivity. That is why most metallic materials, particularly copper and aluminum, have smaller values of intrinsic absorptivity. On the other hand, the apparent (extrinsic) absorptivity at a metal surface is considerably modified by its surface mechanical and chemical properties, such as roughness and oxidation [9, 11]. Therefore, the effective

absorptivity also is a function of the surface condition of the substrate. Increased roughness or oxidation of the metal surface can greatly enhance the coupling of laser energy. In addition to the influence of the electrical resistivity and the surface condition, the absorptivity is related to the laser-beam wavelength [9]. In metals, absorptivity increases for shorter-wavelength laser beam. For example, absorptivity of the polished steel surface is about 30% for Nd:YAG laser with 1.06  $\mu\text{m}$  wavelength, and is six times more than that for  $\text{CO}_2$  laser with 10.6  $\mu\text{m}$  wavelength. If the surface is oxidized, the absorptivity can increase to the value of 60% for  $\text{CO}_2$  laser radiation.

In laser surface alloying and cladding processes, alloy powder has to be used. It is provided by either blowing the powder into the interaction zone or preplacing the powder on the surface of the substrate. In both cases, energy absorption has been observed to be significantly improved.

### **3.5.3.2 Traverse Speed**

Traverse speed is the velocity at which the substrate moves with respect to the stationary laser beam. The ratio of the beam diameter to the traverse speed defines the interaction time. For a given spot size, the reduction in traverse speed increases the interaction time. This will lead to the increase of the dilution, if other variables such as laser-beam power and powder feed rate, are held constant. On the other hand, variation of traverse speed has a marked effect on the dimensions of the cladding tracks. The clad width slightly increases and the clad thickness rapidly increases as the traverse speed decreases. When the power density and powder feed rate are held constant, the traverse speed has an upper and a lower limits. The high speed limit will cause cladding to cease due to insufficient energy input to melt the substrate surface, and low speed limit will

lead to the high dilution or even the distortion of the substrate due to the high energy input. Therefore, for laser cladding process, suitable traverse speed has to be selected to ensure the mechanical properties of the cladding layer and the metallurgical bonding between the clad and the substrate.

### **3.5.3.3 Powder Feeding Techniques**

There are two techniques to supply the alloy powder for laser surface alloying and cladding. One is the preplaced powder technique, and the other is the blown powder technique. The former is called the two-step process, while the latter is called the one-step process.

For two-step process, loose or paste-bound powder is preplaced on the substrate surface before laser irradiation [70-71]. This process was used in the early stages of development of laser surface alloying and cladding. However, two-step process has many drawbacks, such as weak bonding with the substrate, uncontrollable clad thickness, and insufficient operation flexibility, so that it is not suitable for an automatic production environment.

For one-step process, alloy or carbide/metal composite powder is transported by an inert gas stream, usually argon or helium, and injected through a nozzle directly into the center of the laser beam/molten pool on the moving substrate. This method of powder supply is widely used due to its high process quality and flexibility. There are two manners to deliver the alloy powder into the molten pool: laterally injecting the powder into the molten pool [72-73] or injecting the powder into the molten pool through a coaxial nozzle along with the laser beam [74-75]. By using the coaxial nozzle, which was designed by researchers at High Energy Laser Processing Laboratory, Michigan State

University, the efficiency of powder utilization is up to 80%, and the localized areas of components of complex geometry can be deposited with better control on clad thickness and dilution by carefully selecting the processing parameters.

Powder feed rate is defined as the total powder amount supplied per unit time. The variation of powder feed rate greatly affects the clad thickness and dilution. If other variables are held constant, the clad thickness increases linearly, and the dilution decreases with the increase of the powder feed rate.

#### **3.5.3.4 Shielding Gas**

The shielding gas is usually used to protect the optical components from fume and spatter, and thus to ensure effective transmission of the laser beam to the interaction zone. The shielding gas also protects the molten material from oxidation. For laser surface alloying and cladding process, an inert gas such as helium or argon is usually used as the shielding gas. However, since helium gas is expensive, argon gas is used as the shielding gas to reduce the production costs for laser cladding process.

Shielding gas flow rate has a great effect on the clad quality. Increasing the cover gas flow rate helps reduce the dilution of the clad by enhancing cooling rate (other processing parameters remaining constant). However, a high cover gas flow rate leads to the formation of porosity inside the cladding layer due to bubble entrapment. Therefore, the optimum shielding gas flow rate has to be selected to ensure the clad quality.

#### **3.5.4 Advantages of Laser Cladding Process**

Laser surface modification has many advantages over other competing techniques, such as plasma spraying, flame spraying, and tungsten inert gas (TIG) welding. Compared to plasma spraying, the laser process offers a good bonding between the coatings and



substrate, and a lower level of porosity. Compared to TIG welding, the laser surface cladding has the advantage of smoother coating surface, lower dilution, more economic use of expensive alloys, lower thermal distortion, less machining, higher process flexibility, and better suitability for on-line process control and automatic production [76-77].

### **3.5.5 Limitations of Laser Cladding Process**

Laser surface treatment has many advantages, but it has some limitations. A main characteristic of all laser surface treatments is that the treated region is a narrow strip. For this reason, larger surface areas to be treated can be finished only by overlapping tracks. From the point of view of cost-effectiveness, laser surface treatments are suitable for manufacturing costly and special parts. Obviously, it is this reason that limits the wider applications of laser cladding process in consumer product industries.

### **3.5.6 Applications of Laser Cladding Process**

Laser materials processes, such as laser cutting, laser welding, and laser heat treatment, have been successfully implemented in many industrial applications. However, in most cases, laser surface cladding is still in various stages of experimental development. Some real-world applications of laser cladding in industry are described as follows:

It is well recognized that Rolls Royce is a pioneer in taking advantage of the many benefits of laser cladding for production purpose. The first and the most well-known application is the cladding of interlocking edges of turbine blades at Rolls Royce. A Cobalt-based alloy was deposited on the Nickel-based superalloy blades by laser cladding process using a 2 kW CO<sub>2</sub> laser, and the one-step powder feeding technique [78]. Since

then, this new technique has been widely used to rebuild or repair the worn turbine blades and vanes.

Another application introduced by Toyota Motor Company is the laser cladding process for engine valve seats [79]. By this process, the valve seats were directly formed on the cylinder head by cladding copper-based alloy powder on the aluminum substrate. It was reported that the temperature of the valves and their seats was reduced, the overall engine performance was improved, and the durability of the engine was enhanced three times in comparison to the conventional process of the valve seat preparation.

## **Chapter 4**

### **EXPERIMENTAL PROCEDURES**

#### **4.1 General Description**

This research mainly consists of the two parts: one is to develop a simple but realistic model that is relating the maximum clad thickness with process variables, and the other is to deposit hard-facing tracks along complex geometric patterns, onto AISI 1045 (medium carbon) steel roller for fabricating patterned rotary cutting die by laser cladding process.

In this research, designing a powder feeding system, measuring the powder utilization coefficient, and determining the relationship between the clad width and processing parameters, were considered. The practical goal was to determine optimal process parameters for laser cladding of CPM 10V and CPM 15V on AISI 1045 steel plate and roller.

In order to reach this goal, a combination of CAD (computer-assisted design)/CAM (computer-assisted manufacturing) process and a laser cladding system (a laser generator, a beam delivery system, a close-loop powder feeder, a powder-flow splitter, and a special coaxial nozzle) were used to precisely deposit the hard-facing tracks in a preprogramming geometric pattern, onto an AISI 1045 steel roller for fabricating a rotary cutting die

## **4.2 Choice of Materials**

The aim of laser surface cladding is to deposit the intended material with the required mechanical and physical properties on different metallic substrates in order to alter their surface properties, such as wear resistance, corrosion resistance, and high-temperature oxidation resistance. Typically, cost-effective structural materials like plain or mild carbon steel, and aluminum alloy are used as substrates. The clad materials used depend on the application purposes.

### **4.2.1 Substrate Material**

As mentioned in Chapter 1, in the conventional rotary cutting-die process, the entire die block and cutting blades are made of an expensive tool steel D2. In practical application, only cutting blades are used for cutting functions. Therefore, the die block made of tool steel is not necessary, and completely wasteful. Also, the heat treatment cost of tool steel die block is very expensive. In order to greatly reduce the cost of material itself, AISI 1045 medium carbon steel plates and rollers were used as the substrates in this study. The steel plate was used in modeling work, and its dimension was 100 mm x 50 mm x 12 mm. In addition, a steel roller was used for fabrication of the patterned rotary cutting die, and its dimension was 305 mm in length, and 101.6 mm in diameter. The substrate surface was ground to remove oxidation and rust before laser cladding process. For convenience, the chemical compositions of AISI 1045 steel and clad materials are listed in Table 1.

Table 1- Chemical composition of substrate and clad materials (wt. pct)

Materials	Fe	Cr	V	C	Mn	Mo	Si	S
1045 steel	bal.	---	---	0.43-0.5	0.6-0.9	---	---	0.05
CPM 10V*	bal.	5.25	9.75	2.45	0.50	1.30	0.90	0.09
CPM 15V*	bal.	5.25	14.5	3.40	0.50	1.30	0.90	0.07

\* The chemical compositions of CPM 10V and CPM 15V are provided by Crucible Materials Corporation.

#### 4.2.2 Clad Materials

In order to significantly improve the wear resistance of cutting blades and prolong the life of rotary cutting dies, the clad materials used in this research were commercially available tool steel powders, CPM 10V and CPM 15V, which are made by the Crucible Particle Metallurgy (CPM) process. The particle size for CPM 10V was -325 mesh ( $\leq 44 \mu\text{m}$ ), and for CPM 15V was +200 mesh ( $\geq 74 \mu\text{m}$ ). The chemical compositions of CPM 10V and CPM 15V are listed in Table 1.

CPM 10V was designed as a tough, air hardening alloy with added high carbon and vanadium for superior wear resistance, toughness, and strength for cold and warm tooling applications. It is these properties that make it an excellent candidate to replace other conventional wear-resistant materials in cold work tooling applications, particularly where tool toughness is a problem.

CPM 15V contains 50% more hard vanadium carbides in its microstructure than CPM 10V, to provide even higher wear resistance. Therefore, it is intended for applications requiring exceptional wear resistance.

As a result of pronounced ingot segregation, conventional tool steels often contain a coarse, nonuniform microstructure accompanied by inferior mechanical properties along the transverse direction. However, tool steels CPM 10V and CPM 15V produced by the CPM process exhibit very homogeneous microstructures with uniformly dispersed spherical carbides. These steels are characterized by exceptional wear resistance and relatively good impact toughness in comparison with conventional tool steels, such as D2 and M2, as shown in Figures 2 and 3 [80].

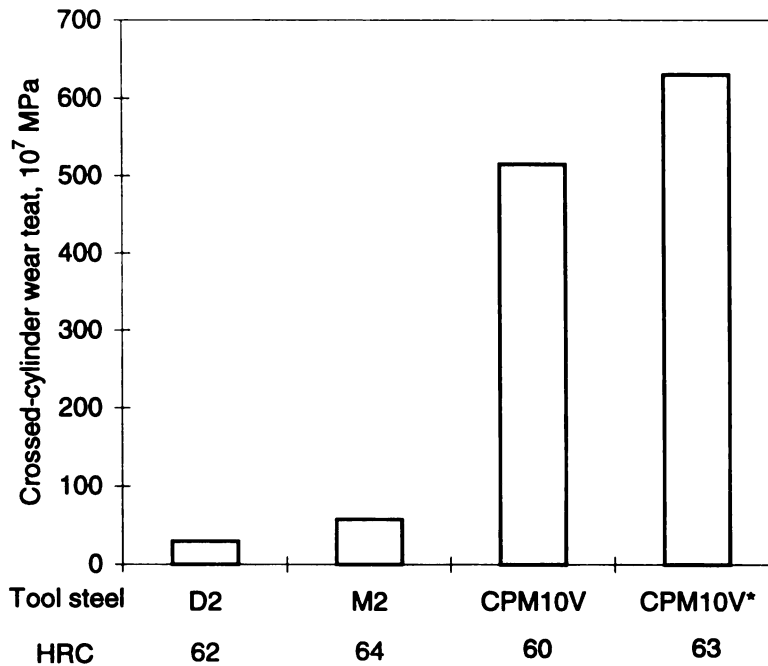


Figure 2- Wear resistance of CPM 10V and conventional tool steels at indicated hardness [80]. CPM 10V\* (hardened) is subjected to quenching, which increases its hardness, and thus the extra wear resistance.

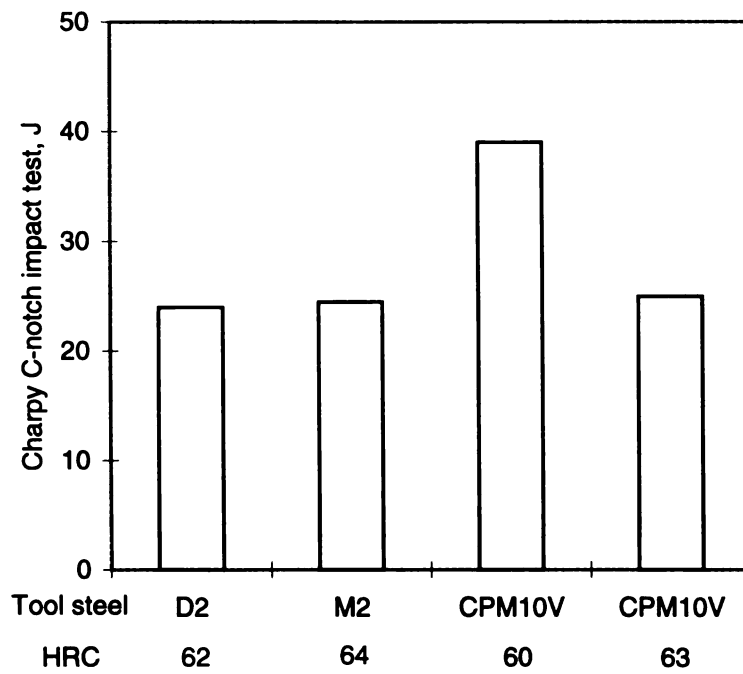


Figure 3- Charpy C-notch impact properties of CPM 10V and conventional tool steels at indicated hardness [80].

### 4.3 Laser Cladding System

Laser cladding system mainly consists of a continuous-wave CO<sub>2</sub> laser, a set of optical mirrors, a powder feeding system, and a computer-assisted manufacturing (CAM) system. The experimental setup is shown in Figure 4.

#### 4.3.1 CO<sub>2</sub> Laser

A continuous wave CO<sub>2</sub> laser operating in the TEM<sub>01</sub>\* mode, with an output power range of 200 to 2500 watts was used for laser cladding experiments. A 2500 L model Triumph (Triumph Industrial Lasers Inc., MA) laser, with the characteristics given in Table 2, was used. For the purpose of this experiment, the laser was operated in a continuous wave (cw) mode.

Table 2- Characteristics of the RF excited CO<sub>2</sub> laser

Parameter	Value/Type
Type of Laser	Fast flow coaxial CO <sub>2</sub> laser
Mode of the beam	TEM <sub>01</sub> *
Output stability	±2%
Beam diameter (raw)	≈ 18 mm
Excitation	RF excited
Temporal mode	Continuous and pulsed (1-10 kHz)
Maximum output power	2800 watts (continuous)
Wave length	10.6 μm
Gas consumption	He: 64 l/hr
	N <sub>2</sub> : 12 l/hr
	CO <sub>2</sub> : 3 l/hr

#### 4.3.2 Beam Delivery System

Optical devices mainly consist of a beam bender mirror and a transmissive ZnSe focal lens with a focal length of 190.5 mm. Laser beam generated by laser machine travels



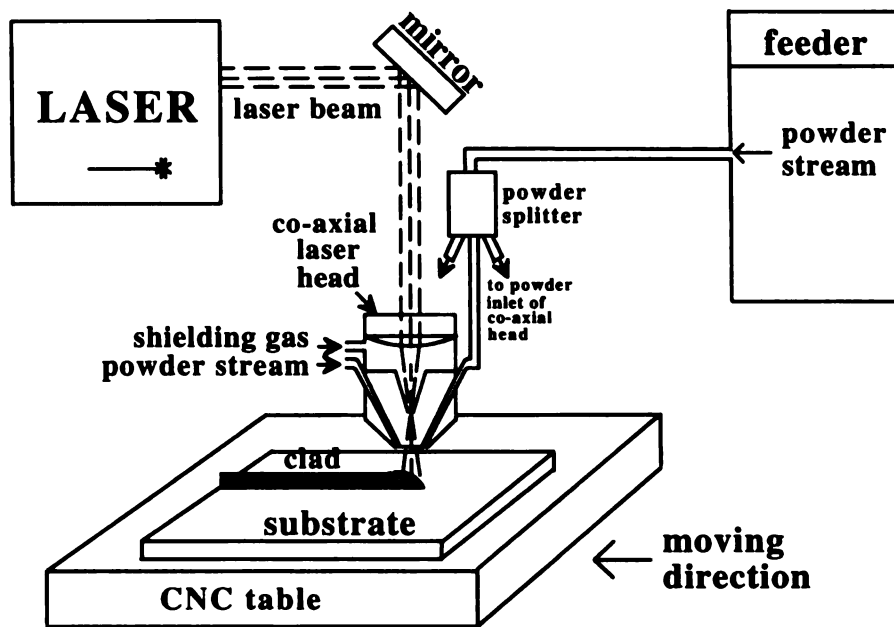


Figure 4- A schematic of laser cladding system.

along its optical axis to a beam bender mirror, then vertically reflects down to a focusing lens, and finally reaches the surface of a substrate for laser treatment process.

#### **4.3.3 Powder Feeding System**

The quality of laser cladding tracks really depends upon the processing variables, and the position, stability, continuity, and accuracy of the powder feeding. Even a small deviation of the powder flow rate, and the location of powder delivered with respect to laser beam center, will lead to a significant variation of the geometry, thickness, and smoothness of the cladding layer.

So far, lateral powder feeding system has been widely used in laser surface alloying and cladding [73, 79]. However, based on our laser cladding experience, such a feeding system has many drawbacks. First, it is difficult to align the location of the powder delivery with respect to the laser beam center because the powder material is brought laterally into the interaction zone. This positioning is very critical, and a small deviation will greatly decrease the powder catchment efficiency (to be defined later), and lead to a bad quality of cladding tracks. With side powder feeding systems, cladding tracks are generally rough, and the thickness and width of tracks are not uniform. Secondly, side feeding system, once set up, might work well for a linear cladding track, i.e., x- or y- motion only, but does not work well for complex geometric patterns requiring bidirectional motions. Typically, the inclination angle between the delivery tube and horizontal plane is 25-35°, and the distance from the delivery tube tip to the interaction zone is 12-15 mm, so the distance from the laser nozzle tip to workpiece requires at least 20 mm, as shown in Figure 5. This gap is so large that shielding gas is not fully able to protect the cladding surface from oxidation. If the cover gas flow rate is

increased, the powder is blown away. For these reasons, it is necessary to develop a new powder feeding system, which produces high stability, continuity, and accuracy of powder flow.

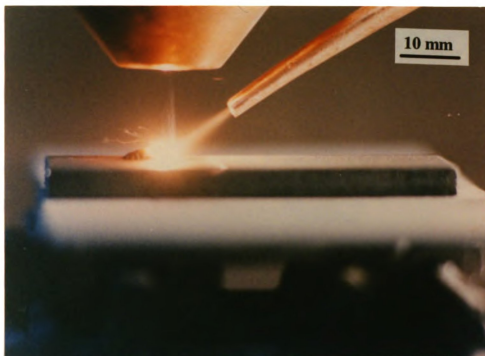


Figure 5- A view of side powder feeding system.

Few publications have reported the design of a nozzle which has a coaxial powder flow [74-75]. However, one of the designs has a main drawback, the powder stream interacts with the laser beam inside the nozzle. As a result, molten or partially molten particles are delivered to the surface of a substrate. Because of this, the nozzle tip frequently clogs up and/or burns out. In our new design, the cone-shaped powder stream (its vertex lies on the specimen surface) interacts with the laser beam just on the surface of a substrate, and therefore the coaxial nozzle (equipped with water-cooling system) performs very well for laser surface alloying and cladding for on-line production. The new powder delivery system designed includes a close-loop powder feeder, a powder splitter, and a coaxial nozzle, as shown in Figure 4.

#### **4.3.3.1 Powder Feeder**

A close-loop powder feeder (METCO model 9MP) was used for providing a stable, continuous, and accurate powder feeding rate. It utilizes a weight-loss metering system to control the powder feed rate. The powder feeder works as a fluidized-bed metering mechanism, and can consistently deliver alloy powder at rates as low as 0.07 gm/sec.

#### **4.3.3.2 Powder-Flow Splitter**

The powder feeder transports the alloy powder, through a hose, to the powder-flow splitter by using pressurized argon gas (called carrier gas). The powder stream is split into four streams of powder flow. These four streams are then carried through four tubes to the coaxial nozzle, where they converge to form a cone-shaped powder stream with the same central axis as the laser beam. This cone of powder finally reaches the laser-generated molten pool on the surface of a workpiece, as shown in Figure 6.

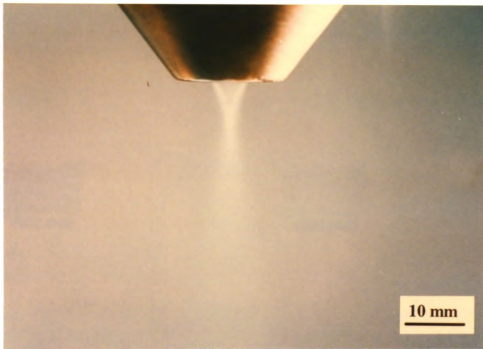


Figure 6- A view of cone-shaped powder stream.

#### 4.3.3.3 Coaxial Nozzle

Figure 7 is a schematic diagram of the transverse section of our coaxial nozzle. The specifications in this diagram were developed by us, based on extensive preliminary investigations in High Energy Laser Processing Laboratory. The final mechanical drawing and actual fabrication of the coaxial nozzle were performed by the Bernal Division of Stevens International.

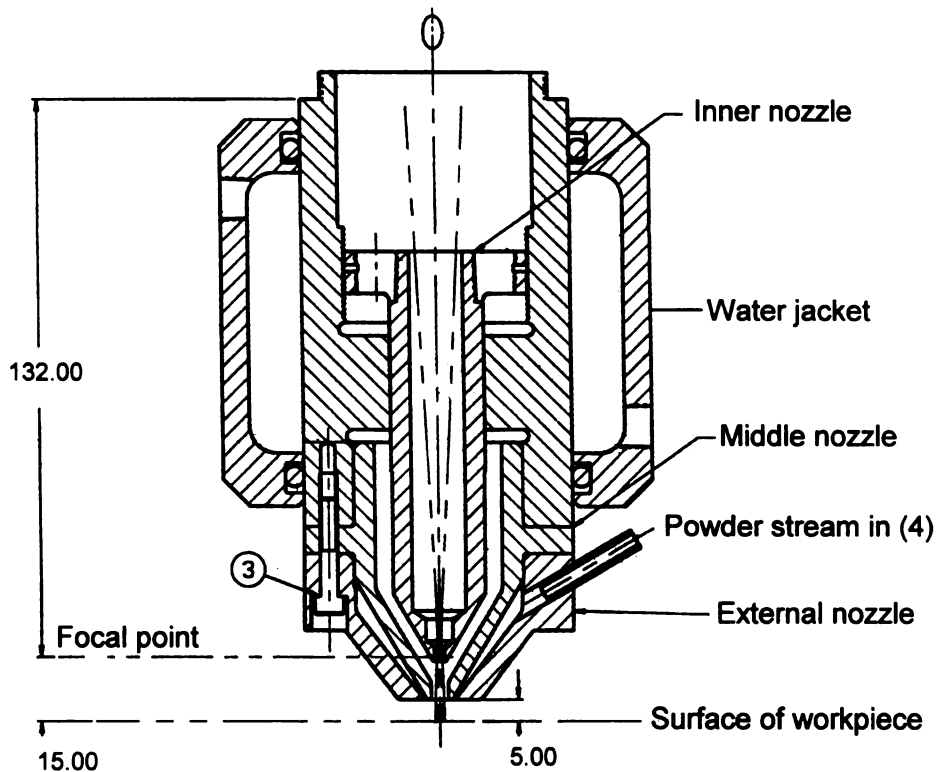


Figure 7- A schematic of the transverse section of a coaxial nozzle.

The coaxial nozzle consists of an inner nozzle, a middle nozzle, an external nozzle and a water jacket for cooling. The inner nozzle has a channel, through which the focused laser beam passes, and it prevents the particles from flowing up the lens by the positive shielding gas pressure.

The middle and the external nozzles form a cone-shaped circumferential channel with  $27^\circ$  cone angle, where four parts of powder streams converge as has been stated before. It should be pointed out that, on the bottom surface, the gap between the middle and external nozzles is really a critical design parameter. If this gap is too large, the powder streams can not converge, and the powder transportation is then by free fall. Another characteristic of this nozzle is that spacers can be inserted to upper place on the middle nozzle for adjusting defocus distance which controls spot diameter. For this coaxial nozzle, the minimum spot size on the specimen surface is 1.8 mm. As shown in Figure 7, the gap from the bottom surface of the coaxial nozzle to the specimen surface is fixed at 5 mm. At this setting, the powder utilization coefficient exceeds 80% (This can be stated as the catchment efficiency of 0.8).

During laser cladding process, a considerable amount of laser radiation is reflected to the bottom surface of the nozzle, and heats the nozzle to a relatively high temperature. Therefore, the circulating-water cooling system is necessary to prevent overheating of the nozzle. From our study, this nozzle, equipped with cooling system, can work very well for a continuous long time use.

This new powder delivery system avoids all of the drawbacks of a lateral powder feeding system. It can provide highly stable, continuous, and accurate powder feed rate, and deliver the powder stream coaxially into the molten pool with the laser beam to form high

quality of cladding tracks, with smooth surface, and uniform thickness and width. Also, this system allows deposition of complex geometric patterns on a flat, or a curved surface for different applications, such as fabrication of rotary cutting dies, repair of turbine blades, and prototyping of forging dies.

#### **4.3.4 CAM System**

Computer-assisted manufacturing (CAM) system was used for laser cladding experiments. CAM system consists of a high precision X-Y table with a computer controller (General Numeric Inc.), and its specifications are given in Table 3. The specimen mounted on X-Y table was translated under a stationary laser beam. The combination of CAM system with two linear axes and step motor was utilized to fabricate rotary cutting dies.

Table 3- CNC machine specifications

Description	Value
Range of motion	1.27 m x 1.27 m
Maximum traverse speed	0.254 m/sec
Maximum contour speed	0.127 m/sec
Accuracy	0.0166 cm/m
Resolution	0.0127 cm
Repeatability	0.00254 cm

#### **4.4 Laser Cladding**

Laser cladding experiments were carried out in two separate sets of experiments: one was to deposit tool steel CPM 10V on AISI 1045 medium carbon steel flat plates for modeling work, and the other was to deposit tool steel CPM 15V on AISI 1045 steel rollers for fabrication of patterned rotary cutting dies.



To date, no published literature has reported that tool steels, CPM 10V and CPM 15V, are used as hard-facing materials for manufacturing plate and rotary cutting dies by laser cladding process. Therefore, wide ranges of experiments were accomplished to measure the powder utilization coefficient, determine the correlation between the clad width and process parameters, develop various relationships between the maximum clad thickness and process parameters, and investigate the optimal process variables for fabricating rotary cutting dies for industrial application.

The main processing parameters important for laser cladding are laser power, laser spot diameter and shape, traverse speed, powder feed rate, and shielding gas flow rate. The process parameters used in this research covered a wide range: Laser power varied from 1.1 to 2.4 kW, laser spot diameter from 1.8 to 3.4 mm, traverse speed from 3 to 14.3 mm/sec, and powder feed rate from 0.1 to 0.25 gm/sec. Argon was used as the shielding gas, and its flow rate was fixed at 1.27 m<sup>3</sup>/hr, which ensured to prevent the deposited coatings from oxidation during laser cladding. The detailed process parameters are given in different sections in order to clearly explain and discuss different relationships.

Laser cladding with injection of powder materials is the most complex case of laser material processes because it is related to numerous process variables, and involves various physical and metallurgical phenomena. Therefore, modeling the laser cladding process is a difficult task. It is not possible to predict the influence of an individual parameter on the whole cladding process. In practice, several parameters have to be varied simultaneously in order to change one characteristic of the deposited layer. For instance, obtaining clads of the same height at different traverse speeds requires to modify

the amount of powder injected into the molten pool and the laser power or the laser spot diameter.

Figure 8 shows an overview of a single cladding track on a AISI 1045 steel flat plate. The cladding track, with 80 mm in length, 4 mm in width, and 1.5 mm in height, is smooth in appearance, and upon testing, found to be metallurgically sound. The process parameters corresponding to this sample are as follows: laser power = 2073 watts, spot size = 3.4 mm, traverse speed = 3.9 mm/sec, powder feed rate = 0.167 gm/sec, and shielding gas (argon) flow rate = 1.27 m<sup>3</sup>/hr.

Figure 9 displays a view of intersecting hard-facing cladding tracks on a AISI 1045 steel roller with 50.8 mm in diameter. The cladding tracks, with smooth surface, uniform thickness and width, were found to have no macrocracks in crossover region. The experimental result showed that the curvature of a substrate has no effect on the quality of circumferential clad formation. Thus, this new process has opened a novel application field of laser surface cladding, through which complex geometric patterns on steel substrates can be deposited for manufacturing cutting and/or stamping dies. The parameters used for the sample shown in Figure 9 are the same as those of the sample mentioned above. Tool steel CPM 10V was used as the hard-facing material. It should be pointed out that, for a middle circumferential cladding track, shielding gas flow rate was increased from 1.27 to 1.7 m<sup>3</sup>/hr, and as result of some of alloy powder was blown away, causing the bad quality cladding track.

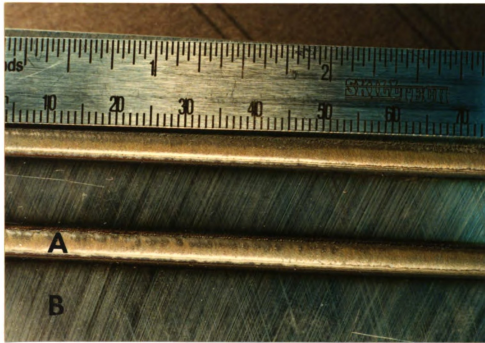


Figure 8- A view of a single cladding track with smooth surface on a steel plate.

(A: clad. B: substrate)

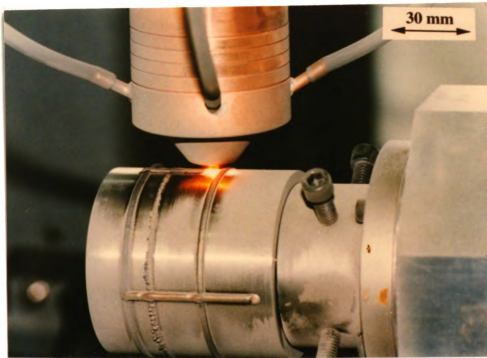


Figure 9- A view of intersecting hard-facing cladding tracks directly deposited on a steel roller.

## **4.5 Post-Clad Treatment**

Tempering treatment was carried out in a bench-top Lindberg 58114 wire element furnace with a microprocessor-base controller. In terms of the heat treatment specification of tool steel CPM 10V, laser cladding samples were double tempered at 540 °C for 15 minutes each, and then cooled to the room temperature. The aim of tempering treatment in this study was to release the thermal stresses caused by laser cladding process.

Subzero treatment was carried out in liquid nitrogen. The tempered sample was dipped into liquid nitrogen for 15 minutes. This treatment led to the transformation of the retained austenite to martensite, and therefore the hardness obviously increased.

## **4.6 Microstructures and Hardness Measurements**

The laser produced samples were sectioned, mounted, polished, and etched using standard metallographic techniques. The microstructures of the cladding layer, interface, and heat-affected zone were characterized by optical microscopy (OM). The equipment used for microstructural observation was given as follows:

- Olympus PM-10AK optical microscope.
- Olympus PME-3 optical microscope.

The microhardness measurements of laser cladding samples under different treatment conditions were carried out using a LECO M-400-G1 microhardness tester. A 1000-g load was used for the measurement, and the indentation time was set at 15 seconds. The hardness measurements were taken across the cladding layer, heat-affected zone, and substrate.

## **Chapter 5**

### **RESULTS AND DISCUSSION**

#### **5.1 Measurement of Powder Utilization Coefficient**

Powder utilization coefficient " $\alpha$ " is defined as the ratio of the amount of powder participating in cladding to the total amount of powder provided by the feeding system within the duration of laser irradiation on the substrate. The value of  $\alpha$  is not only related to the type of feeding mechanism, such as side feeding system or coaxial feeding system, but also to material characteristics like the type of powders, and nature of substrates, etc. Generally, the  $\alpha$  value for coaxial feeding system is much higher than that for side feeding system (typically,  $\alpha$  value falls between about 0.3 and 0.5) due to the precise deposition of the powder with respect to the center of the laser beam.

Other material factors can be divided into intrinsic and extrinsic properties of the clad and substrate materials. Intrinsic properties include thermal conductivity, thermal diffusivity, specific heat, latent heat, reflectivity, and mass density of the powder and the substrate. These intrinsic properties affect the molten-pool temperature, and temperature distribution in the substrate and thereby affecting clad formation. The extrinsic properties include particle size, particle-size distribution, particle shape, and the surface condition of the substrate. A powder suitable for laser cladding must have a proper particle-size distribution and particle shape for it to efficiently absorb laser energy and form a molten pool. Spherical particles are preferable for smooth powder delivery. A large substrate

provides a large heat sink and therefore reduces the pre-heating effect at the laser-molten-pool front. This may lead to the decrease in powder utilization efficiency. As mentioned in Chapter 2, the substrate surface condition has a significant effect on the absorption of the incident laser radiation, and hence affects the clad formation.

For the simple modeling work, CPM 10V alloy powder and AISI 1045 steel plate were used as the hard-facing material and substrate, respectively. Numerous experiments with various process conditions were carried out to measure the powder utilization coefficient  $\alpha$ . The powder utilization coefficient  $\alpha$  was computed by setting a powder feed rate, and then recording the laser scanning time, and weighing the sample before and after laser treatment.

If  $W_1$  = weight of the substrate, and  $W_2$  = total weight of the substrate and the clad, then  $W_c = W_2 - W_1$  is the net clad weight within scanning time. If  $F_p$  = power feed rate, then  $W_p = F_p t$ , which is the total weight of powder delivered within the scanning time "t". The powder utilization coefficient  $\alpha$  is then obtained from:  $\alpha = W_c / W_p$ . The processing parameters used to measure  $\alpha$  value are listed in Table 4.

Based on the results in Table 4, a few conclusions can be made as follows:

- For a given laser power and spot size, when traverse speed varies in a range of about 5 to 10.5 mm/sec,  $\alpha$  value is approximately equal to 0.7 and 0.8 for each process condition, as shown in Figure 10. This shows that  $\alpha$  value is not related to traverse speed.
- For a given laser power, spot size, and traverse speed, when powder feed rate varies from 0.1 to 0.25 gm/sec,  $\alpha$  value is also rather close to 0.8, shown in Figure 11. This means that the ratio  $W_c / F_p$  is a constant when scanning time "t" is fixed because the

net clad weight increases as the increase of powder feed rate. It should be noted that there is a threshold powder feed rate. Poor clad may be produced if powder feed rate is below the threshold due to poor coupling between the powder and the substrate.

- Figure 12 shows that  $\alpha$  value is related to spot size. When laser-beam diameter  $D = 1.8$  mm, average  $\alpha \cong 0.71$ . While  $D \geq 2.3$  mm, average  $\alpha \cong 0.80$ . For convenience, when  $D \geq 2.3$  mm,  $\alpha \cong 0.80$  is employed in this model.

Table 4- Measurements of powder utilization coefficient  $\alpha$

Samples	Power P (watts)	Traverse speed v (mm/sec)	Spot size D (mm)	Powder feed rate F <sub>p</sub> (gm/sec)
A	2073	3.0	2.3	0.167
B	2073	3.9	2.3	0.167
C	2073	4.9	2.3	0.167
D	2073	8.4	2.3	0.167
E	2073	6.6	2.3	0.25
F	2073	8.4	2.3	0.25
G	2073	10.4	2.3	0.25

Samples	Cover gas flow rate (m <sup>3</sup> /hr)	Carrier gas flow rate (m <sup>3</sup> /hr)	Scan time t (sec)	W <sub>1</sub> (gm)	W <sub>2</sub> (gm)
A	1.27	0.51	19.6	89.1344	91.6340
B	1.27	0.51	16.0	91.2466	93.3100
C	1.27	0.51	13.0	87.8486	89.6642
D	1.27	0.51	5.60	80.6674	81.4038
E	1.27	0.51	7.58	82.3200	83.8366
F	1.27	0.51	7.38	103.512	105.005
G	1.27	0.51	4.57	81.4037	82.3500



Table 4 (con'd)

Samples	$W_c=W_2-W_1$ (gm)	$W_p$ (gm)	$\alpha=W_c/W_p$	Average $\alpha$
A	2.50	3.27	0.76	0.80
B	2.06	2.66	0.77	
C	1.82	2.18	0.83	
D	0.74	0.93	0.80	
E	1.52	1.90	0.80	
F	1.49	1.85	0.81	
G	0.95	1.14	0.83	

Samples	Power P (watts)	Traverse speed v (mm/sec)	Spot size D (mm)	Powder feed rate $F_p$ (gm/sec)
H	1567	4.9	1.8	0.1
I	1567	6.6	1.8	0.1
J	2073	6.6	1.8	0.1
K	1567	8.4	1.8	0.1
L	1567	6.6	1.8	0.167
M	1567	8.4	1.8	0.167

Samples	Cover gas flow rate (m <sup>3</sup> /hr)	Carrier gas flow rate (m <sup>3</sup> /hr)	Scan time t (sec)	$W_1$ (gm)	$W_2$ (gm)
H	1.27	0.51	10.40	41.4985	42.2343
I	1.27	0.51	8.33	40.3514	40.9389
J	1.27	0.51	7.42	38.9380	39.4607
K	1.27	0.51	5.95	44.6333	45.0538
L	1.27	0.51	8.33	50.4055	51.4230
M	1.27	0.51	6.31	42.2131	42.9746

Samples	$W_c=W_2-W_1$ (gm)	$W_p$ (gm)	$\alpha=W_c/W_p$	Average $\alpha$
H	0.74	1.04	0.71	0.71
I	0.59	0.83	0.71	
J	0.52	0.74	0.70	
K	0.42	0.60	0.70	
L	1.02	1.39	0.73	
M	0.76	1.05	0.72	

Table 4 (con'd)

Samples	Power P (watts)	Traverse speed v (mm/sec)	Spot size D (mm)	Powder feed rate F <sub>p</sub> (gm/sec)
N	2073	6.6	2.9	0.1
O	2370	8.4	2.9	0.1
P	2073	6.6	2.9	0.167
Q	2370	8.4	2.9	0.167
R	2073	6.6	2.9	0.25
S	2370	8.4	2.9	0.25

Samples	Cover gas flow rate (m <sup>3</sup> /hr)	Carrier gas flow rate (m <sup>3</sup> /hr)	Scan time t (sec)	W <sub>1</sub> (gm)	W <sub>2</sub> (gm)
N	1.27	0.51	7.35	37.5200	38.1130
O	1.27	0.51	5.48	39.2687	39.7213
P	1.27	0.51	7.42	46.4468	47.4229
Q	1.27	0.51	5.12	40.2030	40.8991
R	1.27	0.51	8.03	42.3325	43.9976
S	1.27	0.51	5.95	40.5351	41.7500

Samples	W <sub>c</sub> =W <sub>2</sub> -W <sub>1</sub> (gm)	W <sub>p</sub> (gm)	$\alpha$ =W <sub>c</sub> / W <sub>p</sub>	Average $\alpha$
N	0.61	0.74	0.82	0.82
O	0.45	0.55	0.82	
P	0.98	1.23	0.80	
Q	0.70	0.85	0.82	
R	1.67	2.01	0.83	
S	1.22	1.49	0.82	

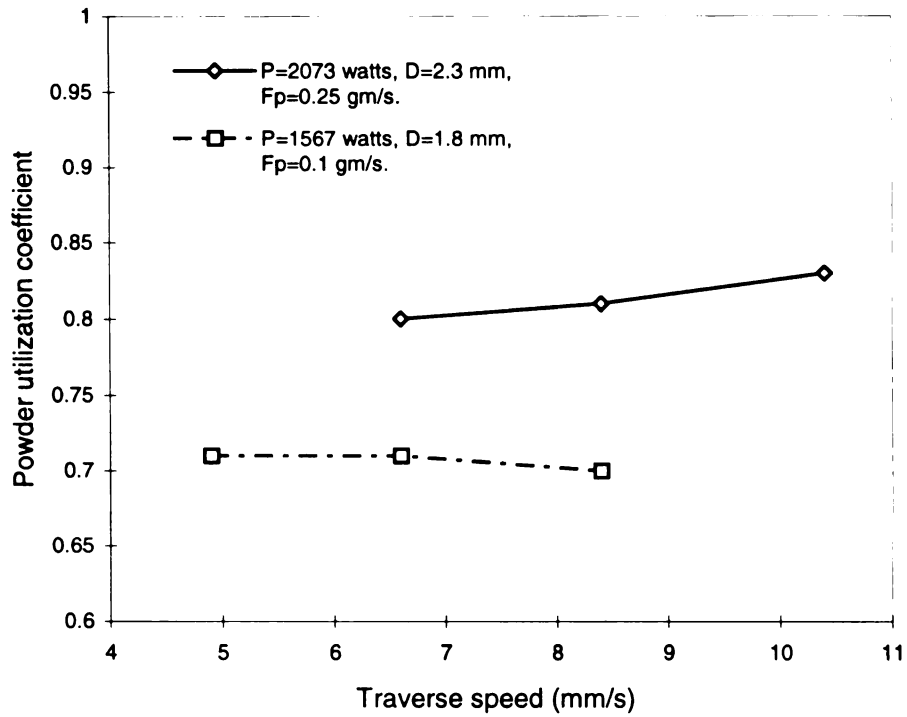


Figure 10- Plot of powder utilization coefficient vs. traverse speed.

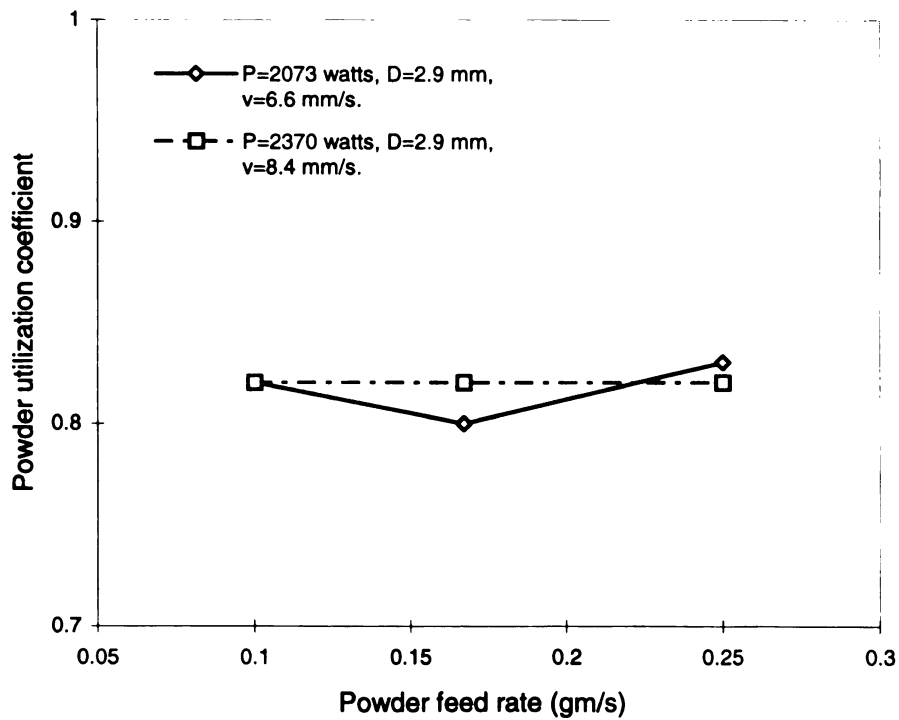


Figure 11- Plot of powder utilization coefficient vs. powder feed rate.

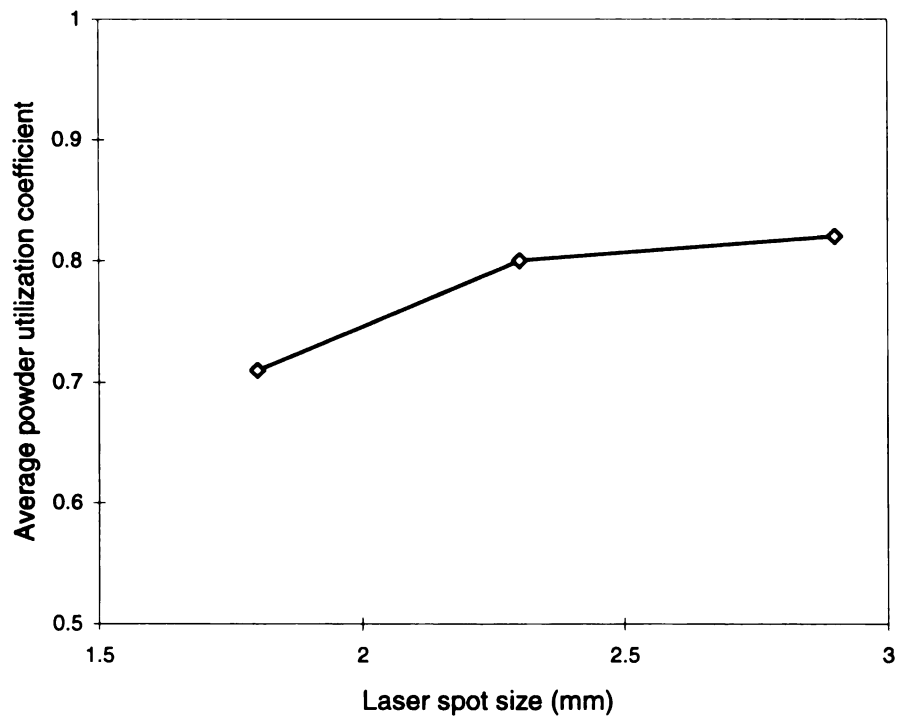


Figure 12- Plot of average powder utilization coefficient vs. laser spot size.

## 5.2 Relationships between Clad Width and Process Parameters

Theoretically, clad width is primarily dictated by the optical configuration which is defined by laser-beam diameter, integrated beam diameter or scanning beam amplitude. However, the clad width is also related to traverse speed, power density, and powder feed rate. In order to determine the relationship between the clad width and processing parameters, many experiments were carried out under various process conditions. The process variables and experimental results are listed in Table 5.

Based on the results in Table 5, we can make some conclusions:

- With other variables held constant, clad width modestly decreases as the traverse speed increases, as seen in Figure 13. When traverse speed accelerates to about 9 mm/sec, clad width is almost equal to laser-beam diameter. This speed is called threshold traverse speed. Below threshold traverse speed, the clad is wider than spot size. For this speed range, the average clad width is used to calculate the maximum clad thickness. Thus, laser-beam diameter is substituted for the clad width, in the model, when traverse speed varies from ~8.5 to ~14.5 mm/sec .
- Clad width gently increases with the increase in energy density when other parameters are kept constant, as shown in Figure 14. This is because sufficient energy is available to melt material situated at a distance wider than the beam itself.
- With other variables held constant, the clad gently widens as powder feed rate increases, as shown in Figure 15. If the energy input is sufficient, the large powder feed rate will lead to a wider clad track.

Table 5- Correlation between clad width and processing parameters

Samples	Power P (watts)	Traverse speed v (mm/sec)	Spot size D (mm)	Powder feed rate F <sub>p</sub> (gm/sec)	Cover gas flow rate (m <sup>3</sup> /hr)
1	2073	3.0	2.3	0.167	1.27
2	2073	3.9	2.3	0.167	1.27
3	2073	4.9	2.3	0.167	1.27
4	2073	5.8	2.3	0.167	1.27
5	2073	6.6	2.3	0.167	1.27
D	2073	8.4	2.3	0.167	1.27
F	2073	8.4	2.3	0.25	1.27
G	2073	10.4	2.3	0.25	1.27

Samples	Carrier gas flow rate (m <sup>3</sup> /hr)	Energy density E <sub>d</sub> (J/mm <sup>2</sup> )	Clad width W (mm)	$\beta=W/D$	Average $\beta$
1	0.51	382.5	3.45	1.50	1.40
2	0.51	294.3	3.35	1.46	
3	0.51	234.2	3.25	1.41	
4	0.51	197.9	3.12	1.36	
5	0.51	173.9	3.00	1.30	
D	0.51	136.6	2.38	1.03	1.03
F	0.51	136.6	2.38	1.03	1.01
G	0.51	110.3	2.30	1.00	

Table 5 (con'd)

Samples	Power P (watts)	Traverse speed v (mm/sec)	Spot size D (mm)	Powder feed rate F <sub>p</sub> (gm/sec)	Cover gas flow rate (m <sup>3</sup> /hr)
H	1567	4.9	1.8	0.1	1.27
I	1567	6.6	1.8	0.1	1.27
K	1567	8.4	1.8	0.1	1.27
6	2073	3	1.8	0.167	1.27
7	2073	3.9	1.8	0.167	1.27
8	2073	4.9	1.8	0.167	1.27
9	2073	5.8	1.8	0.167	1.27
10	2073	6.6	1.8	0.167	1.27
M	1567	8.4	1.8	0.167	1.27

Samples	Carrier gas flow rate (m <sup>3</sup> /hr)	Energy density E <sub>d</sub> (J/mm <sup>2</sup> )	Clad width W (mm)	$\beta=W/D$	Average $\beta$
H	0.51	226.2	2.15	1.19	1.15
I	0.51	167.9	2.00	1.11	
K	0.51	132.0	1.80	1.00	1.00
6	0.51	488.8	3.27	1.82	1.64
7	0.51	376	3.14	1.74	
8	0.51	299.3	3.00	1.67	
9	0.51	252.8	2.80	1.56	
10	0.51	222.2	2.56	1.42	
M	0.51	132.0	2.05	1.14	1.14

Table 5 (con'd)

Samples	Power P (watts)	Traverse speed v (mm/sec)	Spot size D (mm)	Powder feed rate F <sub>p</sub> (gm/sec)	Cover gas flow rate (m <sup>3</sup> /hr)
11	2073	3	2.9	0.167	1.27
12	2073	3.9	2.9	0.167	1.27
13	2073	4.9	2.9	0.167	1.27
14	2073	5.8	2.9	0.167	1.27
15	2073	6.6	2.9	0.167	1.27
16	2073	3.9	2.9	0.25	1.27
17	2073	4.9	2.9	0.25	1.27
18	2073	5.8	2.9	0.25	1.27
19	2073	3.9	2.9	0.1	1.27
20	2073	4.9	2.9	0.1	1.27
21	2073	5.8	2.9	0.1	1.27
Q	2370	8.4	2.9	0.167	1.27
S	2370	8.4	2.9	0.25	1.27

Samples	Carrier gas flow rate (m <sup>3</sup> /hr)	Energy density E <sub>d</sub> (J/mm <sup>2</sup> )	Clad width W (mm)	$\beta=W/D$	Average $\beta$
11	0.51	303.4	3.55	1.22	1.14
12	0.51	233.4	3.40	1.17	
13	0.51	185.7	3.30	1.14	
14	0.51	156.9	3.20	1.10	
15	0.51	137.9	3.11	1.07	
16	0.51	233.4	3.87	1.33	1.27
17	0.51	185.7	3.68	1.27	
18	0.51	156.9	3.55	1.22	
19	0.51	233.4	3.34	1.15	1.09
20	0.51	185.7	3.20	1.10	
21	0.51	156.9	3.00	1.03	
Q	0.51	123.9	2.97	1.02	1.02
S	0.51	123.9	3.03	1.04	1.04



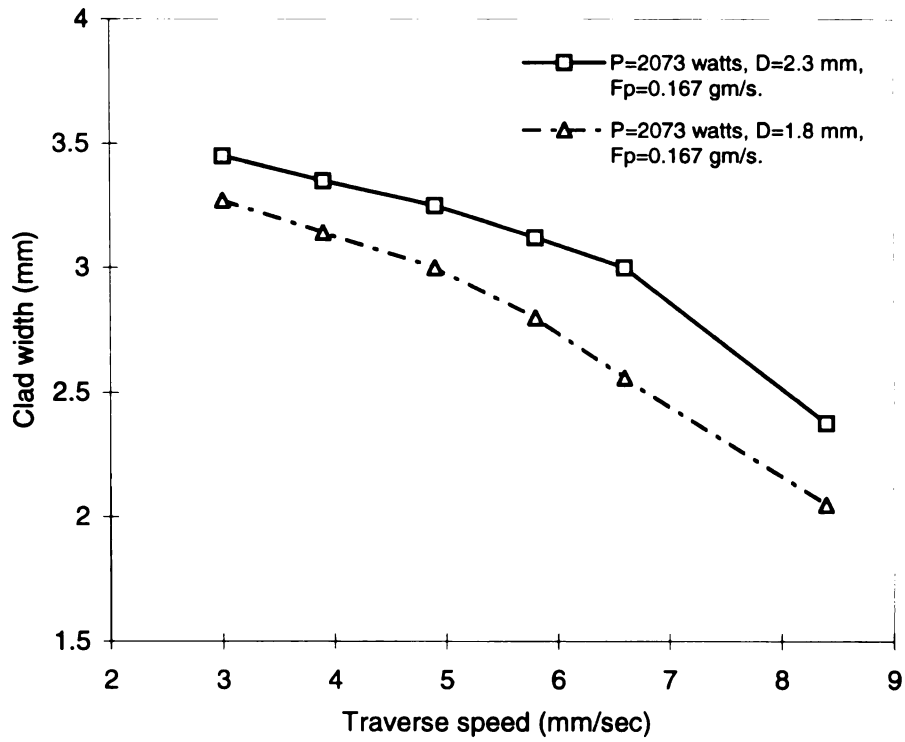


Figure 13- Clad width as a function of traverse speed.

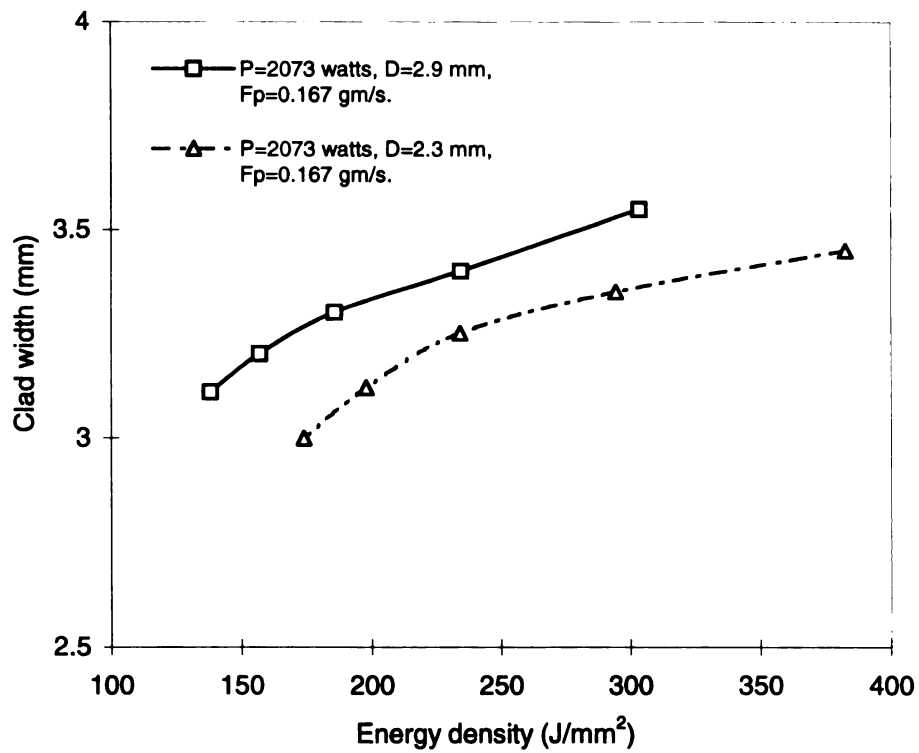


Figure 14- Clad width as a function of energy density.

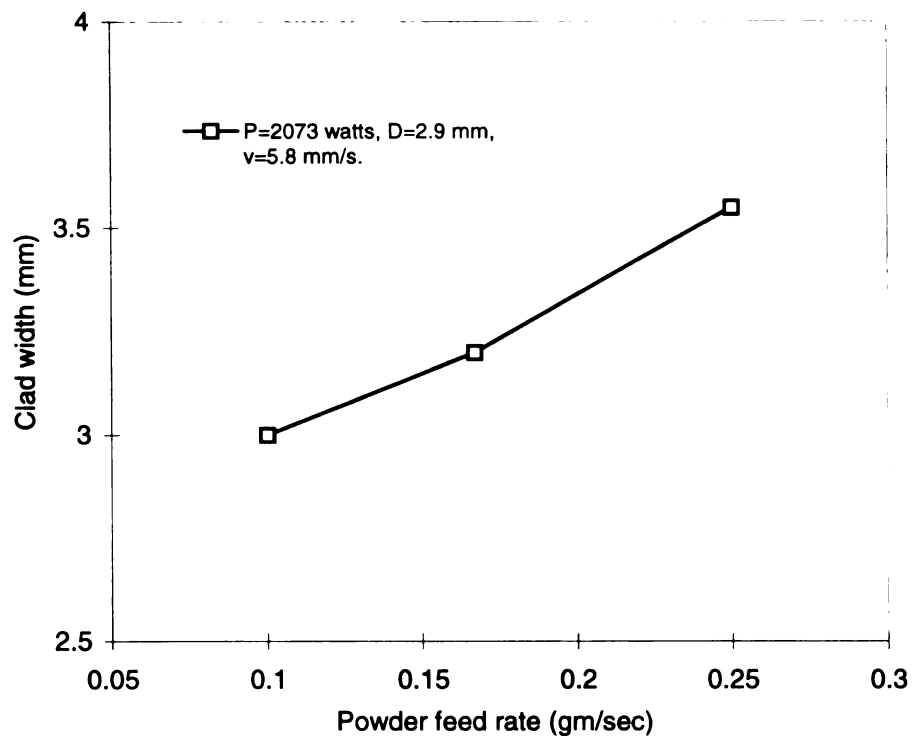


Figure 15- Clad width as a function of powder feed rate.

### 5.3 Process Modeling

The laser cladding is a very complicated process involving the following physical and metallurgical phenomena: (1) laser-beam energy and material interaction; (2) heat transfer in the clad, and the substrate; (3) rapid melting and solidification; and (4) clad material and substrate material reaction and inter-diffusion. For this reason, process modeling of the laser-cladding process is a difficult task. The following model is developed based on the geometric features of the cross section of the clad, physical properties of alloy powder itself, and process parameters. Therefore, the model is based on simple but realistic approximations, and can be used to evaluate the optimal processing conditions for on-line production and manufacturing.

#### 5.3.1 Assumptions

The following model is based on the assumption that power density or energy density is suitable for laser cladding process, where the clad track is sound and free of cladding defects, such as porosity, microcracks, poor metallurgical bond, and high dilution.

#### 5.3.2 Basic Equation

Net clad weight is a function of powder utilization coefficient, powder feed rate, and irradiation time, so it can be expressed as

$$W_c = \alpha F_p t, \quad (1)$$

where  $W_c$  = net clad weight (gm),  $\alpha$  = powder utilization coefficient,  $F_p$  = powder feed rate (gm/sec), and  $t$  = irradiation time (sec) (related to scanning speed).

For simple modeling work, CPM 10V alloy powder is used as the hard-facing material. As discussed earlier, the laser-spot diameter  $D \leq 2$  mm, we measured  $\alpha \cong 0.70$ , while for  $D \geq 2.3$  mm,  $\alpha \cong 0.80$ .

For a single clad track, we assume that the cross-section is approximately represented by a parabolic arch, as shown in Figure 16, and its area is expressed as

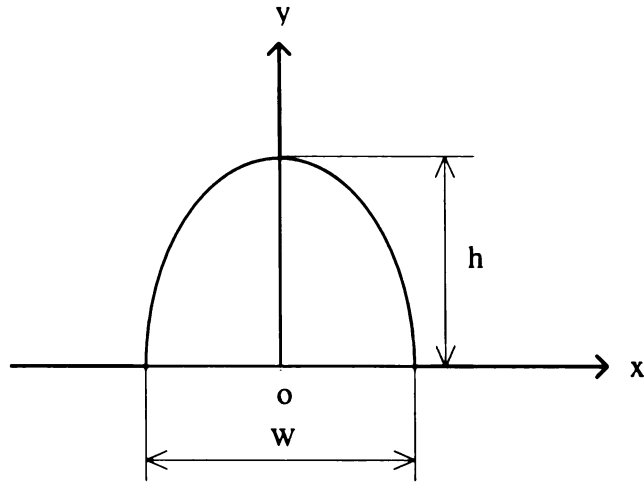


Figure 16- Parabolic shape of the cross-section of a clad track

$$A = \frac{2}{3}wh, \quad (2)$$

where  $w$  = track width (mm) (assume to be equal to the spot diameter), and  $h$  = the maximum clad thickness (mm).

From geometric shape of a clad track, and physical properties of the alloy itself, the net clad weight can be written as

$$W_c = \frac{2}{3} wh(vt)\rho , \quad (3)$$

where  $w$  = clad width (mm),  $v$  = traverse speed (mm/sec),  $\rho$  = alloy density (gm/cm<sup>3</sup>), and  $t$  = irradiation time (sec). For CPM 10V,  $\rho = 7.418$  gm/cm<sup>3</sup>. The term  $\frac{2}{3} wh(vt)$  is actually the volume of a cladding track.

Combination of Eq. (1) and Eq. (3), we can get

$$\frac{2}{3} whv\rho = \alpha F_p . \quad (4)$$

Equation (4) is a basic equation, relating the maximum clad thickness and various process parameters.

### 5.3.3 Energy Density Equation

Energy density or specific energy is defined as [81]

$$E_d = P_d \tau , \quad (5)$$

where  $E_d$  = energy density (J/mm<sup>2</sup>),  $P_d$  = power density (watts/mm<sup>2</sup>), and  $\tau$  = time (sec) required to move a distance of the laser beam diameter along the traverse direction.

Power density is expressed as

$$P_d = \frac{P}{A_1} , \quad (6)$$

where  $P$  = laser power (watts), and  $A_1$  = irradiation area (mm<sup>2</sup>).

For simplicity, assume that the shape of laser spot is circular (for our TEM<sub>01</sub>\* mode laser beam, the shape actually is toroid), then irradiation area  $A_1 = \pi D^2 / 4$ , where  $D$  = laser beam diameter (mm).

Substituting  $A_1$  in Eq. (6), we can obtain

$$P_d = \frac{4P}{\pi D^2}. \quad (7)$$

The time  $\tau$  can be expressed as

$$\tau = \frac{D}{v}. \quad (8)$$

Substituting Eqs. (7) and (8) in Eq. (5), one has

$$E_d = \frac{4}{\pi} \frac{P}{Dv}. \quad (9)$$

The above equation shows that the energy density is directly proportional to laser power, and inversely proportional to spot size or traverse speed.

#### 5.3.4 Clad Thickness-Energy Density Equation

Eqs. (4) and (9) can be rewritten as, respectively,

$$h = \frac{3\alpha F_p}{2wv\rho}, \quad (10)$$

$$\frac{1}{Dv} = \frac{\pi E_d}{4P}. \quad (11)$$

For simplicity, assume that  $w = D$  when  $v \geq 8.4$  mm/sec, then substitute Eq. (11) in Eq. (10), we can obtain

$$h = \frac{3\pi}{8} \frac{\alpha F_p}{P\rho} E_d, \quad (12)$$

where  $\alpha$  = powder utilization coefficient,  $F_p$  = powder feed rate (gm/sec),  $P$  = laser power (watts), and  $\rho$  = alloy density (gm/cm<sup>3</sup>).

For a particular alloy powder, if laser power and powder feed rate are fixed, the clad thickness is directly proportional to energy density, which depends on the spot size and traverse speed.

## 5.4 Correlation Derived from Basic Equation

Equation (10)

$$h = \frac{3\alpha F_p}{2wv\rho},$$

shows that clad thickness is related to powder feed rate, spot size ( $w = D$ , when  $v \geq 8.4$  mm/sec), and traverse speed, while the laser power is held constant. We will discuss it in details.

### 5.4.1 Relationship between Clad Thickness and Traverse Speed

In equation (10), for a given powder (fixed  $\rho$ ), if powder feed rate and spot size are kept constant, then equation (10) can be simplified as

$$h = \frac{C_1}{v}, \quad (13)$$

where  $C_1$  is a constant depending upon process variables and alloy density.

Equation (13) shows that the clad thickness is inversely proportional to traverse speed. The faster the traverse speed, the less is the powder input per unit length, and therefore the thinner the clad track. Under different experimental conditions, the linear relationship between the clad thickness and the reciprocal of traverse speed is shown in Figure 17.

### 5.4.2 Relationship between Clad Thickness and Spot Size

For fixed powder feed rate and traverse speed, equation (10) can be reduced to

$$h = \frac{C_2}{D}, \quad (14)$$

where  $C_2$  is a constant for the assumed conditions.

Equation (14) shows that clad thickness is inversely proportional to the spot size. The larger the spot size, the wider is the clad track, but the thinner is the clad track, as shown in Figure 18.

### 5.4.3 Relationship between Clad Thickness and Powder Feed Rate

If the spot size and traverse speed are kept constant, and then Eq. (10) becomes

$$h = C_3 F_p, \quad (15)$$

where  $C_3$  is a constant which is related to process parameters and alloy density.

Equation (15) reveals that clad thickness and powder feed rate have a linear relation, as shown in Figure 19. The larger the powder feed rate, the more is the powder input per unit length, and the higher the clad thickness. However, for a fixed energy density, if the powder feed rate is too high, it is possible to cause lack of fusion in cladding layer, and produce poor metallurgical bond between cladding layer and substrate.



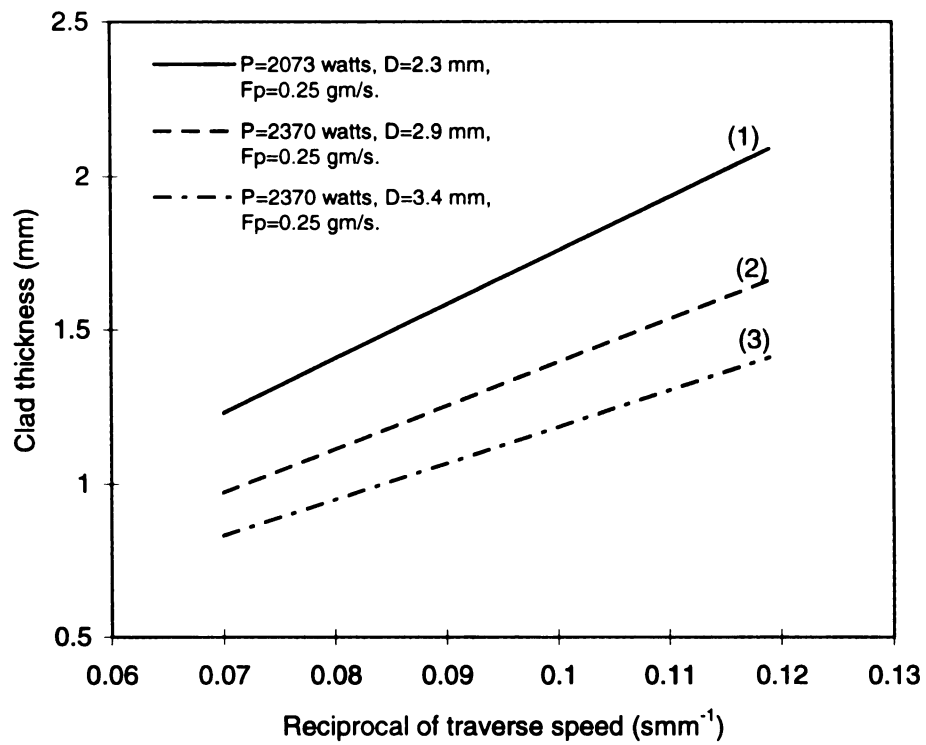


Figure 17- Clad thickness as a function of reciprocal of traverse speed.

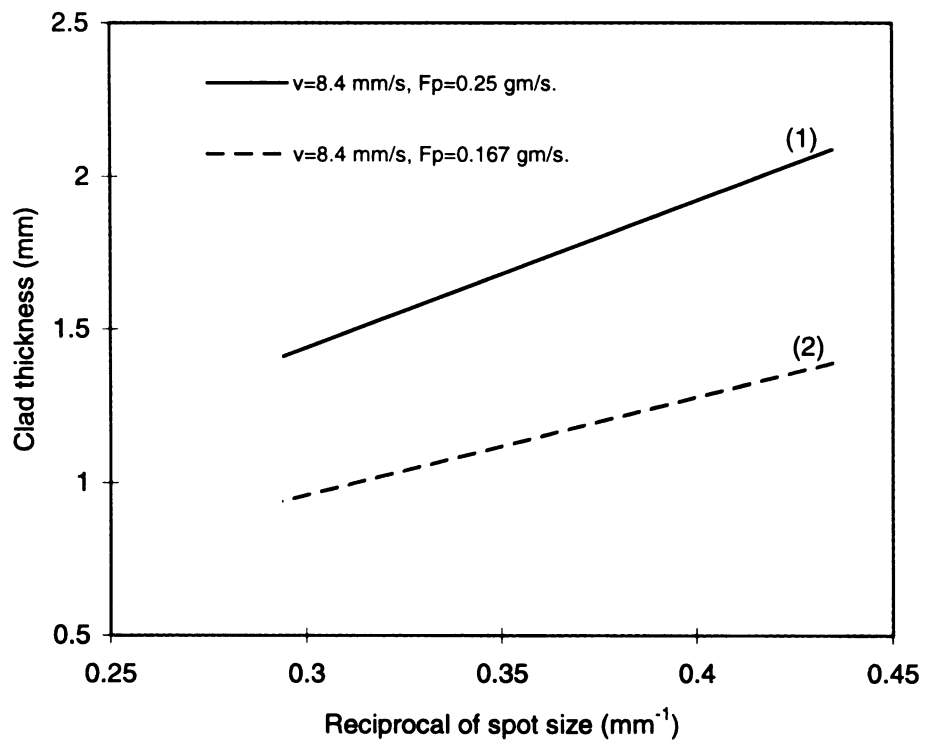


Figure 18- Clad thickness as a function of reciprocal of spot size.

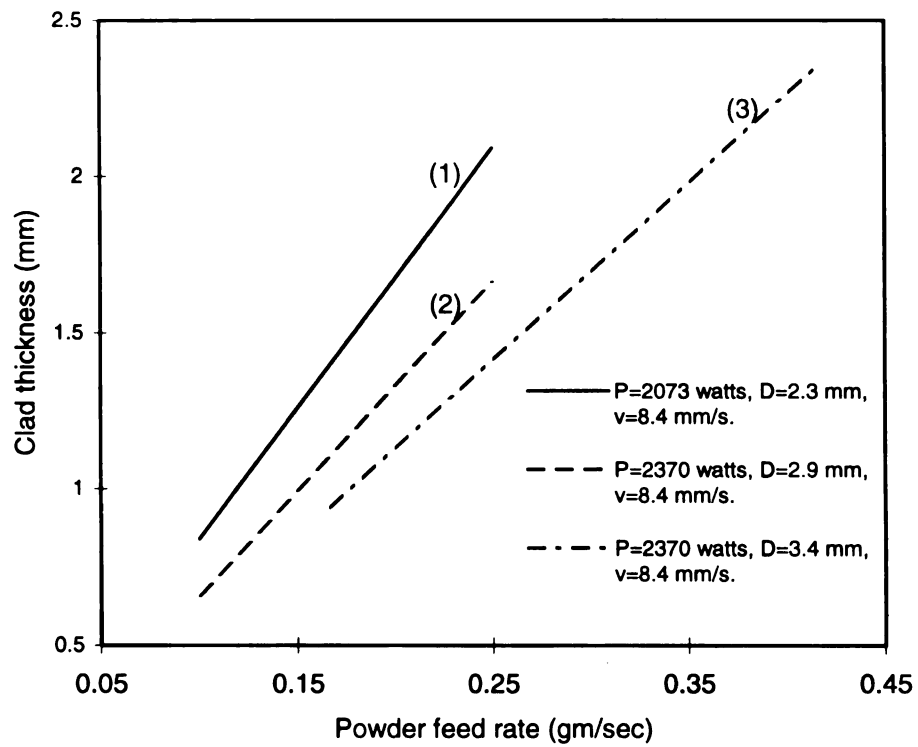


Figure 19- Clad thickness as a function of powder feed rate.

## 5.5 Correlation Derived from the Energy Density Equation

Equation (9) displays that the energy density is related to spot size, laser power, and traverse speed.

### 5.5.1 Relationship Between Energy Density and Spot Size

The laser power and traverse speed are kept constant, and then Eq. (9) is simplified as

$$E_d = \frac{C_4}{D}, \quad (16)$$

where  $C_4$  is a constant.

Equation (16) displays that energy density is inversely proportional to spot size. In other words, energy density and the reciprocal of the spot size have a linear relation, as shown in Figure 20. For very low values of energy density, it is possible to create cladding defects, such as lack of fusion and poor metallurgical bonding, or even debonding. This is because insufficient energy is available to melt the substrate surface after melting powder particles.

### 5.5.2 Relationship between Energy Density and Traverse Speed

When the laser power and spot size are fixed, Eq. (9) is reduced to

$$E_d = \frac{C_5}{v}, \quad (17)$$

where  $C_5$  is a constant.

The above equation demonstrates that the energy density is inversely proportional to traverse speed. The faster the traverse speed, the less the interaction time or dwell time, and the smaller the energy density. The relation between energy density and the reciprocal

of traverse speed is displayed in Figure 21. It shows that energy density linearly increases as the reciprocal of traverse speed increases.

In terms of equation (7), when laser power is fixed, power density is related to spot size, and not related to traverse speed. Therefore, it is more reasonable to use energy density to explain phenomena that happen during laser cladding than power density.

### **5.5.3 Relationship between Energy Density and Laser Power**

If spot size and traverse speed are held constant, then Eq. (9) becomes

$$E_d = C_6 P, \quad (18)$$

where  $C_6$  is a constant.

Equation (18) shows that energy density and laser power have a linear relation. The higher the laser power, the larger the energy density, as shown in Figure 22. If the energy density is too high, it is possible to create high dilution which can change the properties of cladding layer. This is because, for a given powder feed rate, greater energy delivered per unit area causes greater substrate melting and change in clad alloy composition.

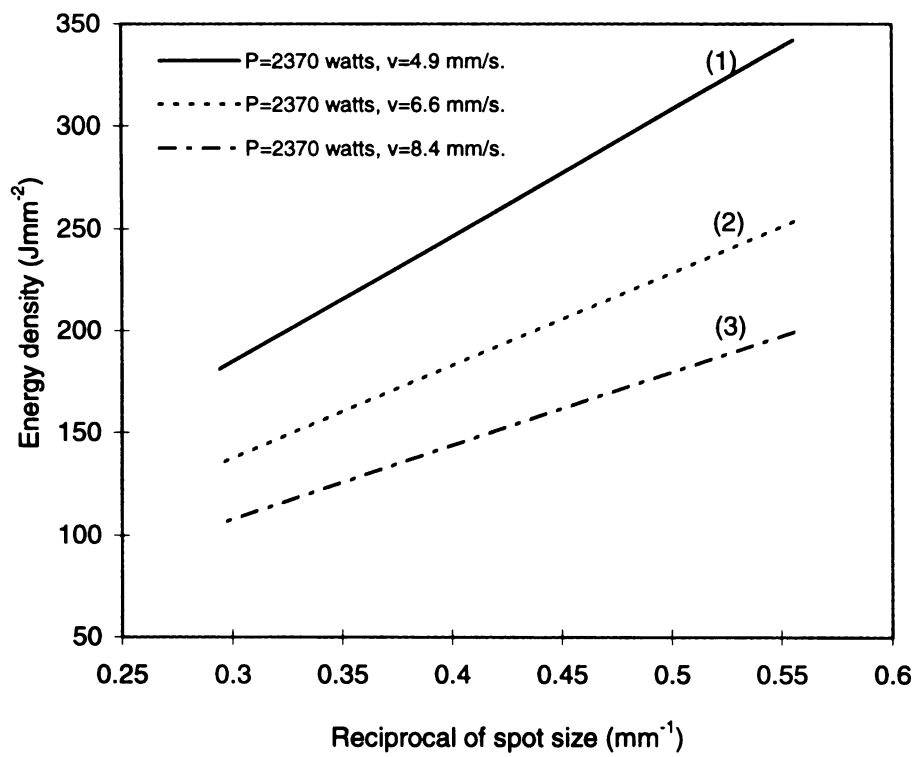


Figure 20- Energy density as a function of reciprocal of spot size.

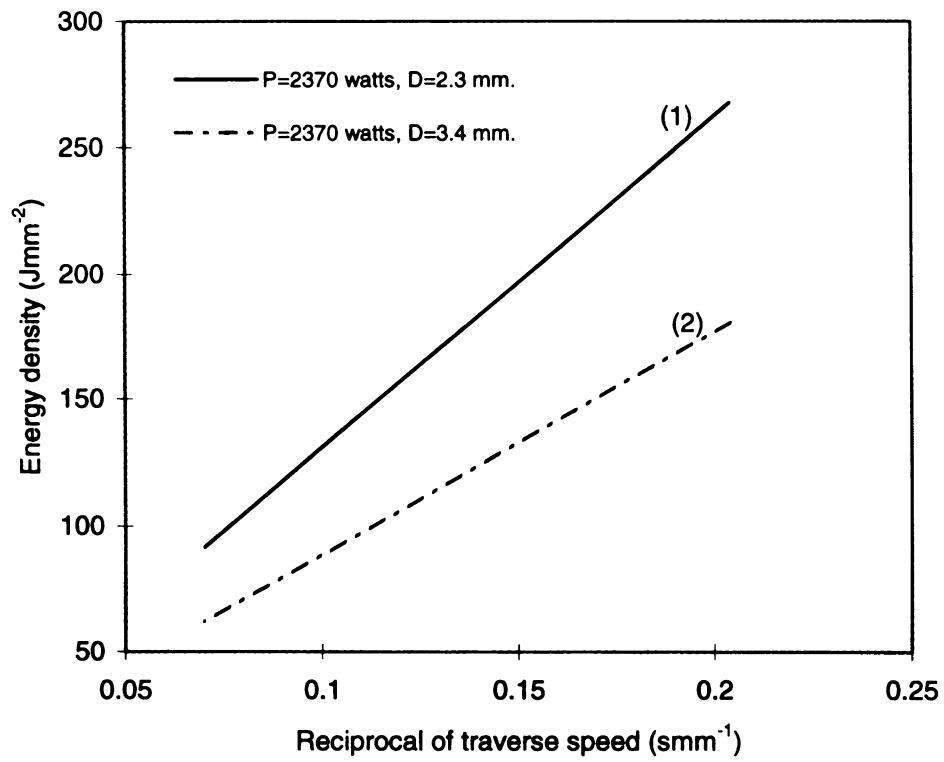


Figure 21- Energy density as a function of reciprocal of traverse speed.

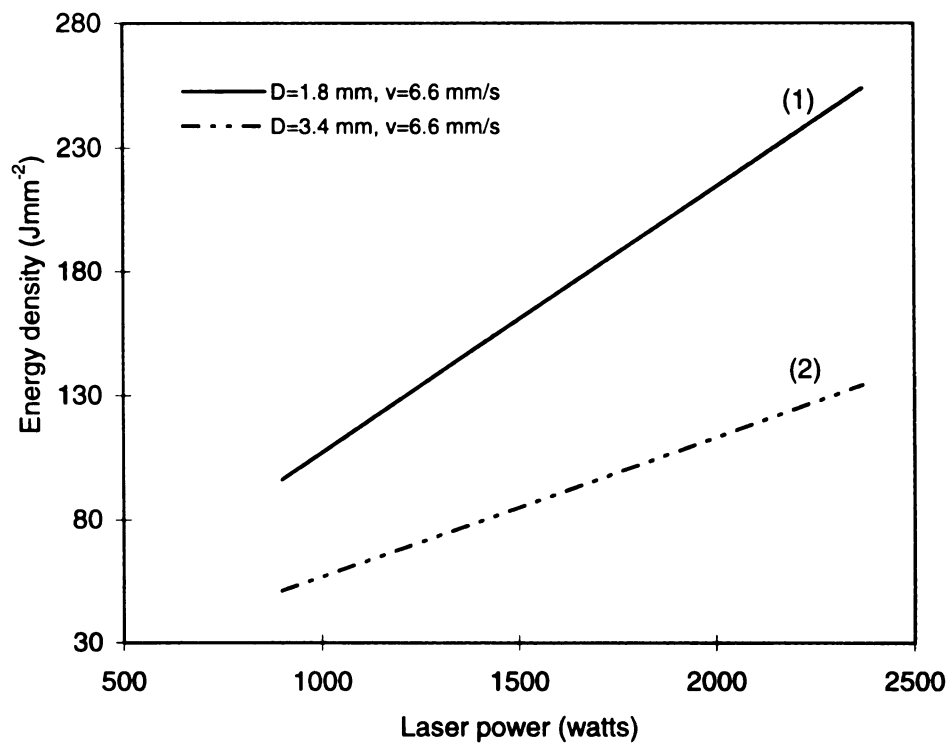


Figure 22- Energy density as a function of laser power.



## 5.6 Correlation between Clad Thickness and Energy Density

Equation (12) displays that clad thickness is related to powder feed rate and energy density, which is subjected to spot size and traverse speed when laser power is fixed. We will discuss the following case.

From equations (13) and (17), we know that, for fixed powder feed rate and spot size, clad thickness is only a function of traverse speed. While, for fixed laser power and spot size, energy density is a function of traverse speed. Therefore, the clad thickness and energy density linearly vary with reciprocal of traverse speed. The faster the traverse speed, the lower the energy density, and thinner the clad track, as shown in Figure 23.

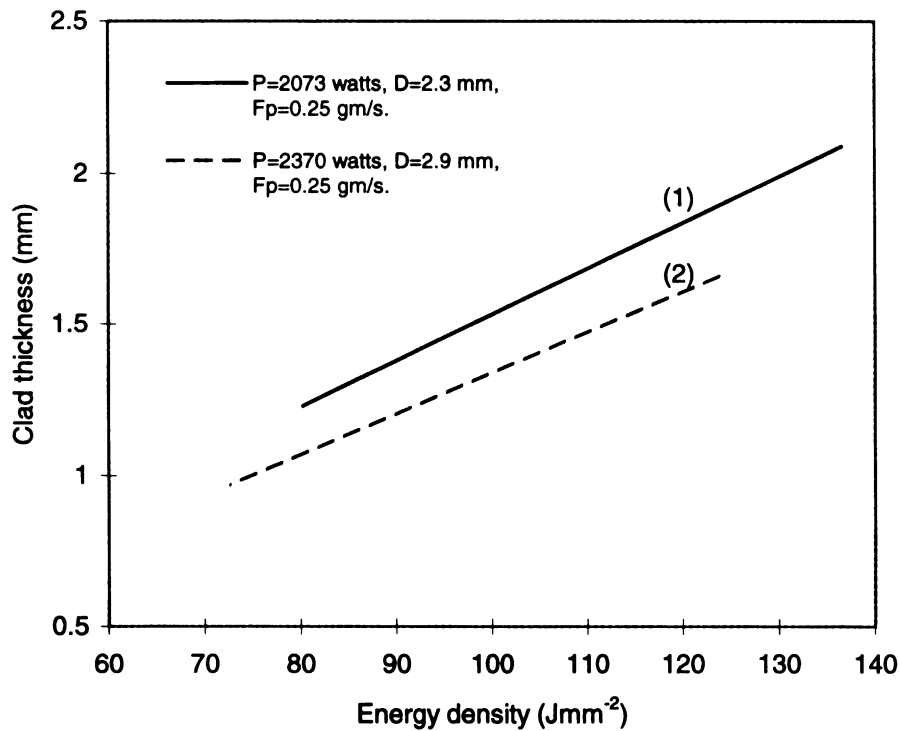


Figure 23- Clad thickness as a function of energy density.

## 5.7 Comparison of Calculated and Experimental Results

To test the validity of this model, its predictions have to be compared with the experimental results of laser cladding. For this reason, many experiments in various process conditions were carried out to verify this model. Laser power varied from about 1000 to about 2400 watts, and spot size from ~2 to ~3.5 mm, traverse speed from ~3.0 to ~14 mm/sec, and powder feed rate from 0.1 to 0.25 gm/sec. In each process condition, the experimental results are in good agreement with those predicted by this simple model.

### 5.7.1 Clad Thickness and Traverse Speed

As mentioned before, when the traverse speed  $v < 8.4$  mm/sec, average clad width is used to calculate clad thickness in equation (10). When traverse speed varies from 8.4 to 14.3 mm/sec, the spot diameter is used to substitute for clad width. The process variables and experimental results are listed in Table 6.

When  $v < 8.4$  mm/sec, inserting the relevant data in Table 6 into equation (10), one can get a equation:  $h = 8.11/v$ , which shows that clad thickness is inversely proportional to traverse speed. Calculated and experimental plots are shown in Figure 24 a. The slope of the calculated plot is 8.11, and the slope of the experimental plot is 6.24. Clad thickness linearly increases with the increase of reciprocal of traverse speed, and experimental and calculated results match very well.

When  $v \geq 8.4$  mm/sec, predicted and experimental plots are shown in Figure 24 b. In both cases, clad thickness also linearly varies with reciprocal of traverse speed, and the calculated result is in good agreement with the experimental result.

Table 6- Processing parameters used to develop the correlation  
between clad thickness and reciprocal of speed

Samples	Power P (watts)	Traverse speed v (mm/sec)	Spot size D (mm)	Clad width W (mm)	Powder feed rate F <sub>p</sub> (gm/sec)
6	2073	3.0	1.8	2.95	0.167
7	2073	3.9	1.8	2.95	0.167
8	2073	4.9	1.8	2.95	0.167
9	2073	5.8	1.8	2.95	0.167
10	2073	6.6	1.8	2.95	0.167
D6	2370	8.40	3.4		0.25
D7	2370	10.4	3.4		0.25
D8	2370	12.5	3.4		0.25
D9	2370	14.3	3.4		0.25

Samples	Energy density E <sub>d</sub> (J/mm <sup>2</sup> )	Cover gas flow rate (m <sup>3</sup> /hr)	Carrier gas flow rate (m <sup>3</sup> /hr)	Clad thickness h (mm)	
6	488.8	1.27	0.51	2.35	2.39
7	376.0	1.27	0.51	1.87	1.91
8	299.3	1.27	0.51	1.57	1.60
9	252.8	1.27	0.51	1.36	1.40
10	222.2	1.27	0.51	1.21	1.23
D6	105.6	1.27	0.51	1.29	1.33
D7	85.3	1.27	0.51	1.08	1.10
D8	71.0	1.27	0.51	0.89	0.97
D9	62.0	1.27	0.51	0.80	0.84

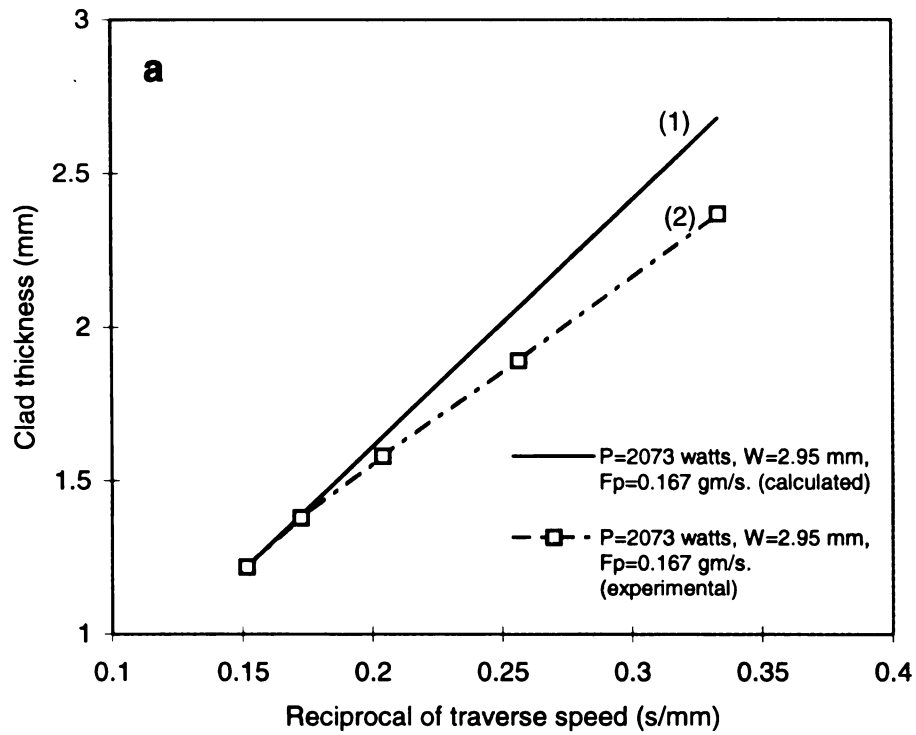
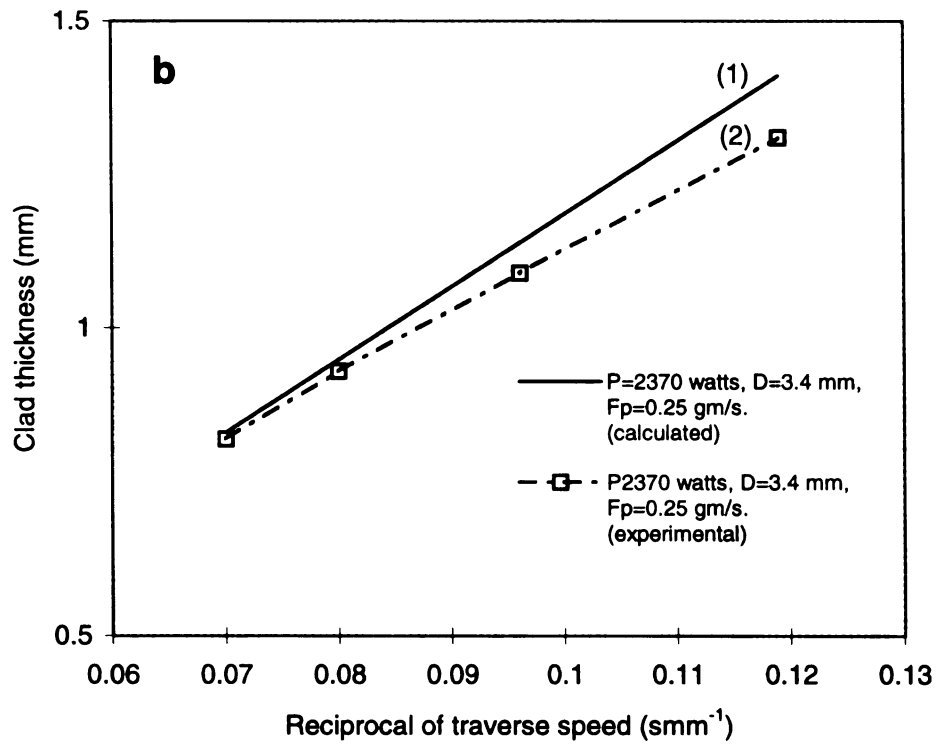


Figure 24- Comparison of calculated and experimental relationship between clad thickness and reciprocal of traverse speed.  
 (a).  $v < 8.4$  mm/sec. (b).  $v \geq 8.4$  mm/sec.

Figure 24 (con'd)



### 5.7.2 Clad Thickness and Spot Size

For fixed traverse speed and powder feed rate, clad thickness is inversely proportional to spot size, as described in equation (14). The process variables and experimental results are given in Table 4. In terms of the relevant data in Table 7, predicted and experimental plots are shown in Figure 25. As seen in Figure 25, clad

thickness linearly increases with the increase of reciprocal of spot size. In other words, the larger the spot size, the thinner the clad track. Also, the predicted and experimental results match reasonably well.

Table 7- Processing parameters used to develop the correlation between cladding thickness and reciprocal of spot size

Samples	Power P (watts)	Traverse speed v (mm/sec)	Spot size D (mm)	Powder feed rate F <sub>p</sub> (gm/sec)
F	2073	8.4	2.3	0.25
S	2370	8.4	2.9	0.25
D6	2370	8.4	3.4	0.25

Samples	Energy density E <sub>d</sub> (J/mm <sup>2</sup> )	Cover gas flow rate (m <sup>3</sup> /hr)	Carrier gas flow rate (m <sup>3</sup> /hr)	Clad thickness h (mm)	
F	136.6	1.27	0.51	1.70	1.75
S	123.8	1.27	0.51	1.47	1.50
D6	105.6	1.27	0.51	1.29	1.33

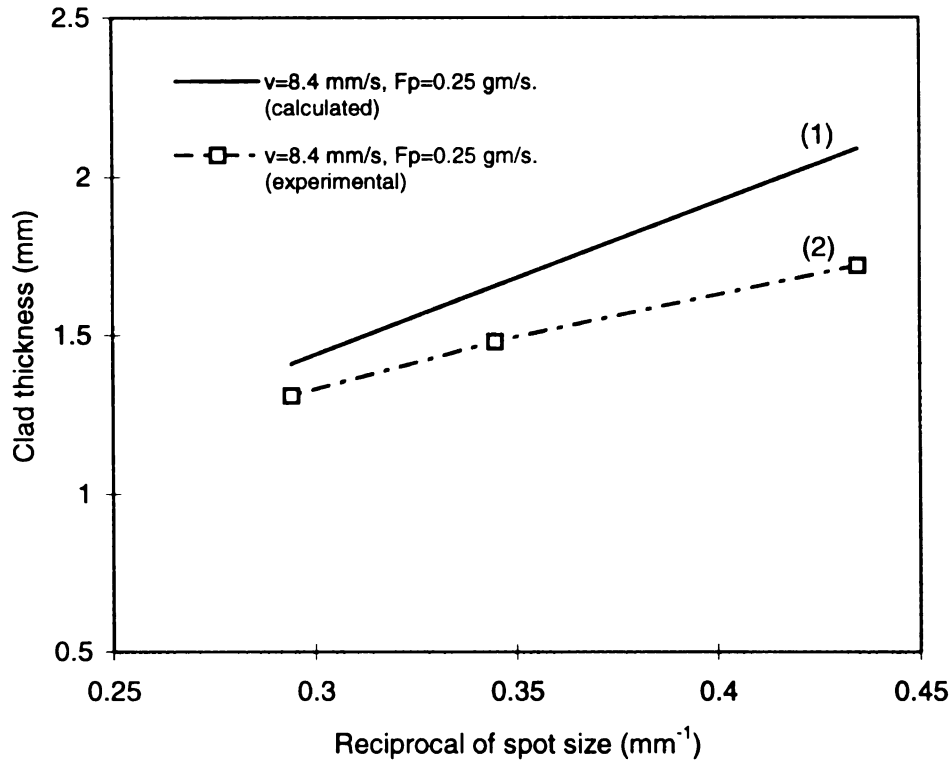


Figure 25- Comparison of calculated and experimental relationship between clad thickness and reciprocal of spot size.

### 5.7.3 Clad Thickness and Powder Feed Rate

If spot size and traverse speed are kept constant, equation (15) shows that clad thickness is directly proportional to powder feed rate. The process parameters and experimental results are listed in Table 8. Inserting the related value in Table 8 in equation (15), its corresponding plot (1) is displayed in Figure 26, while experimental plot (2) in Figure 26. As shown in Figure 26, clad thickness linearly increases as powder feed rate increases.

Table 8- Processing parameters used to develop the correlation  
between clad thickness and powder feed rate

Samples	Power P (watts)	Traverse speed v (mm/sec)	Spot size D (mm)	Powder feed rate $F_p$ (gm/sec)
O	2370	8.4	2.9	0.1
Q	2370	8.4	2.9	0.167
S	2370	8.4	2.9	0.25

Samples	Energy density $E_d$ (J/mm <sup>2</sup> )	Cover gas flow rate (m <sup>3</sup> /hr)	Carrier gas flow rate (m <sup>3</sup> /hr)	Clad thickness h (mm)	
O	123.8	1.27	0.51	0.60	0.64
Q	123.8	1.27	0.51	0.96	1.04
S	123.8	1.27	0.51	1.47	1.50



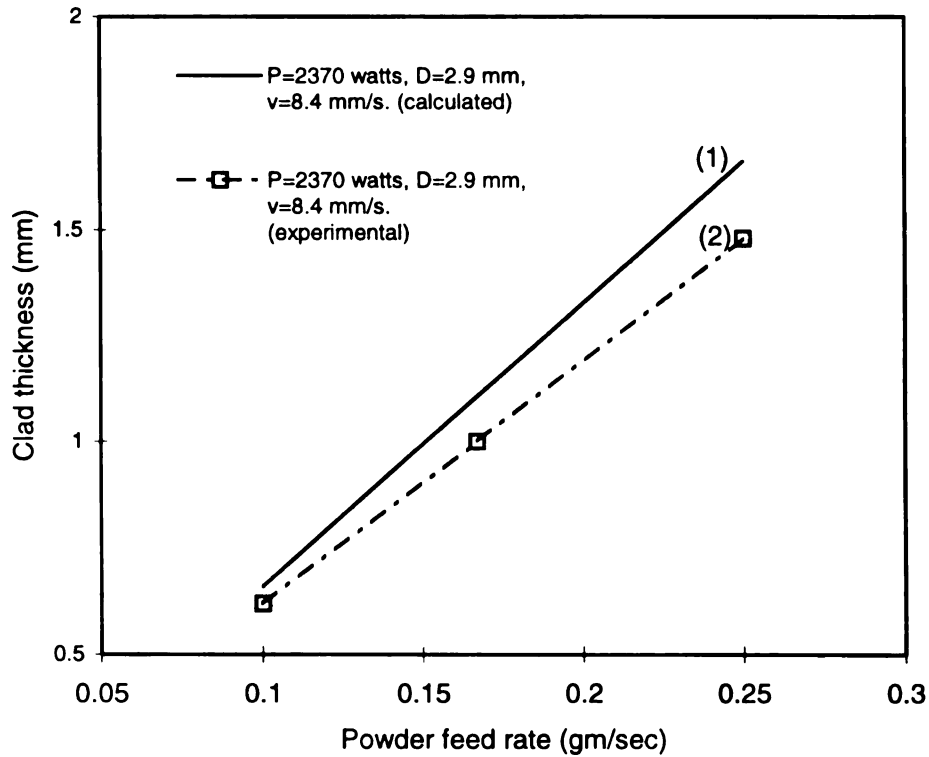


Figure 26- Comparison of calculated and experimental relationship between clad thickness and powder feed rate.

#### 5.7.4 Clad Thickness and Energy Density

Based on the process variables and experimental results listed in Table 9, plots (1) and (2) in Figure 27 shows that calculated and experimental results between the clad thickness and energy density, respectively. Figure 27 shows that the clad thickness and energy density have a linear relationship, as discussed in section 5.6. Also, Figure 27 shows that the calculated result is in good agreement with experimental result.

Table 9- Processing parameters used to develop the correlation between clad thickness and energy density

Samples	Power P (watts)	Traverse speed v (mm/sec)	Spot size D (mm)	Powder feed rate F <sub>p</sub> (gm/sec)
F	2073	8.4	2.3	0.25
G	2073	10.4	2.3	0.25
B5	2073	12.5	2.3	0.25
B6	2073	14.3	2.3	0.25

Samples	Energy density E <sub>d</sub> (J/mm <sup>2</sup> )	Cover gas flow rate (m <sup>3</sup> /hr)	Carrier gas flow rate (m <sup>3</sup> /hr)	Clad thickness h (mm)	
F	136.6	1.27	0.51	1.70	1.75
G	110.3	1.27	0.51	1.47	1.50
B5	91.8	1.27	0.51	1.14	1.16
B6	80.2	1.27	0.51	1.00	1.02

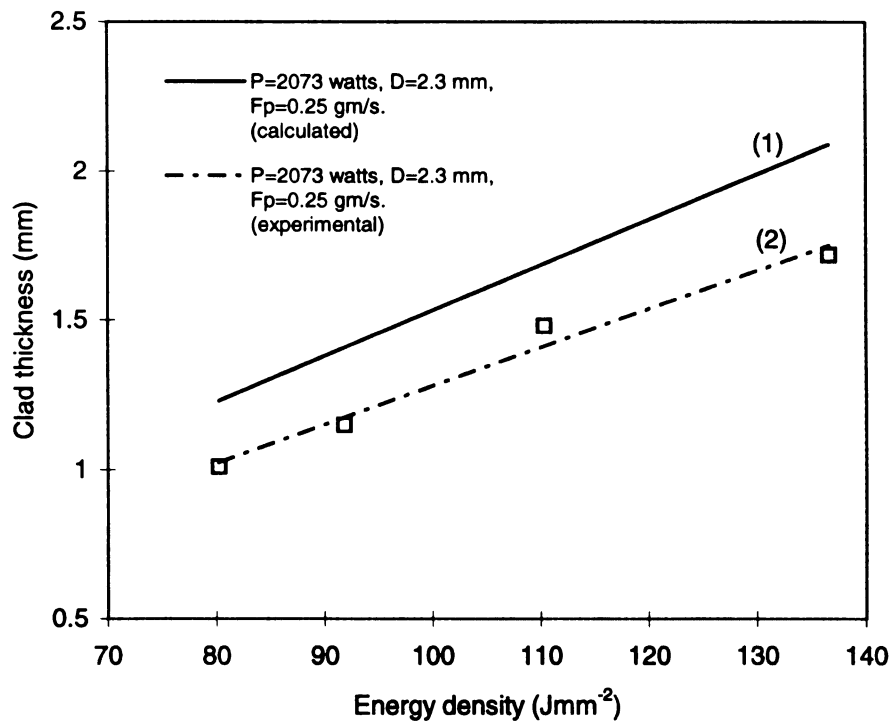


Figure 27- Comparison of calculated and experimental relationship between clad thickness and energy density.

## 5.8 Correlation between Penetration Depth and Energy Density

If traverse speed and spot size in equation (9) are kept constant, energy density is only a linear function of laser power. For a given powder feed rate, the higher is the laser power, the higher is the energy density, thus more energy is transferred to the substrate, and therefore the deeper is the heat-affected zone. Process variables and experimental results are listed in Table 10, and the plot of penetration depth versus energy density is shown in Figure 28. The penetration depth linearly increases with increase in power density. When laser power decreases to about 1000 watts, energy density is so low ( $73.2 \text{ J/mm}^2$ ) that lack of fusion between the cladding layer and the substrate is observed. The corresponding energy density is called the threshold energy density in this particular cladding system. Energy density has to be higher than the threshold energy density to ensure a good metallurgical bonding with the substrate.

Table 10- Processing parameters used to develop the correlation between penetration depth and energy density

Samples	Power P (watts)	Traverse speed v (mm/sec)	Spot size D (mm)	Powder feed rate $F_p$ (gm/sec)
D	2073	8.4	2.3	0.167
31	1755	8.4	2.3	0.167
32	1567	8.4	2.3	0.167
33	1110	8.4	2.3	0.167

Samples	Energy density $E_d$ ( $\text{J/mm}^2$ )	Cover gas flow rate ( $\text{m}^3/\text{hr}$ )	Carrier gas flow rate ( $\text{m}^3/\text{hr}$ )	Penetration depth $h_p$ (mm)
D	136.6	1.27	0.51	0.62
31	115.7	1.27	0.51	0.60
32	103.3	1.27	0.51	0.58
33	73.2	1.27	0.51	0.53

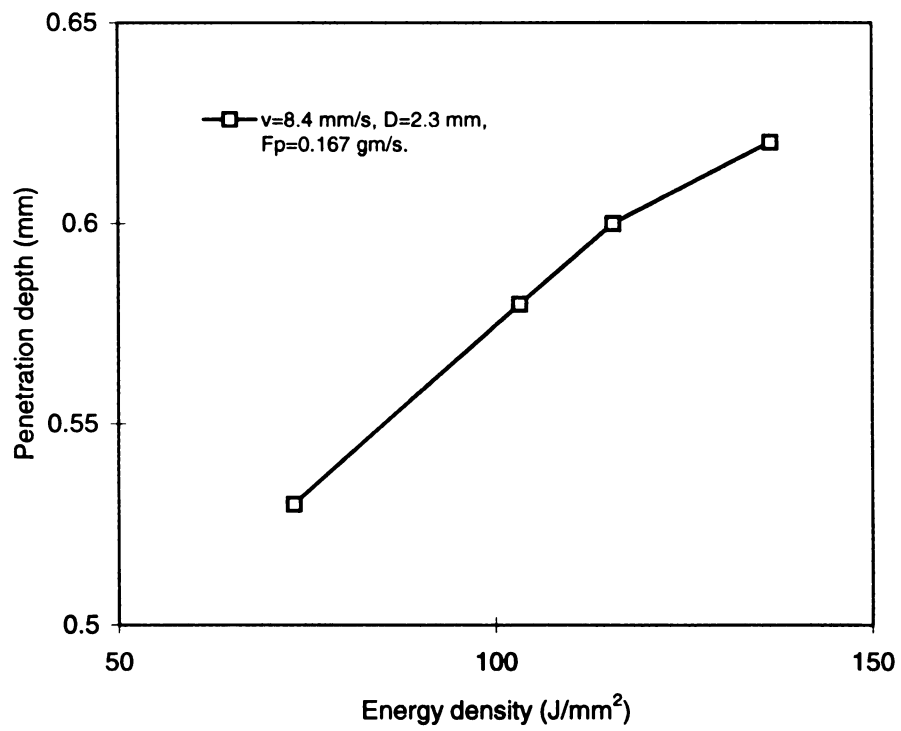


Figure 28- Penetration depth as a function of energy density.

## **5.9 Microstructure**

One outstanding feature of laser cladding process is rapid melting and subsequently rapid solidification. The resultant phases in cladding layers therefore are usually metastable. By laser cladding process, the high cooling rate may extend the metastable solubility, refine the grain size, and form unique nonequilibrium microstructures different from those predicted from the equilibrium-phase diagram. Therefore, the wear-resistant, corrosion-resistant, and oxidation-resistant properties of the treated materials can be attained depending on clad material.

### **5.9.1 Geometric Characteristics of A Single Cladding Track**

The clad bead geometry is related to process parameters, such as power density, traverse speed, and powder feed rate. Figure 29 shows three basic single clad bead profiles. The deep penetration bead, as shown in Figure 29 (a), is produced at a higher power density and/or lower powder feed rate. The bead with a very low dilution and a reasonable width to height aspect ratio can be achieved with the correct balance among power density, traverse speed, and powder feed rate, as shown in Figure 29 (b). This shape allows multiple clad layers to be built up by overlapping single clad track for producing composite material layers and prototyping complicated geometric parts. Parabolic bead with a minimum dilution is produced at higher powder feed rate and/or lower traverse speed, as shown in Figure 29 (c).

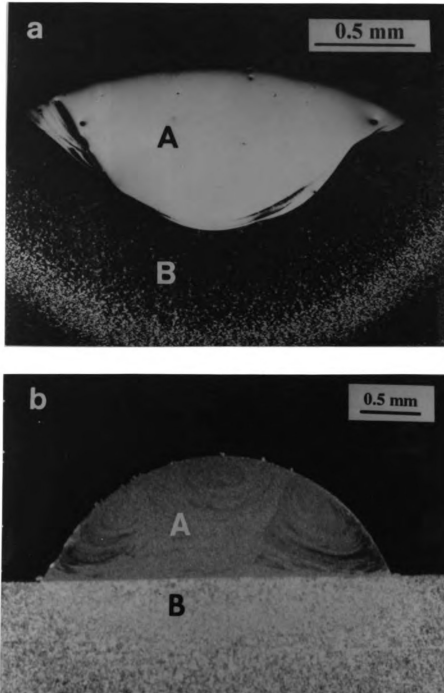
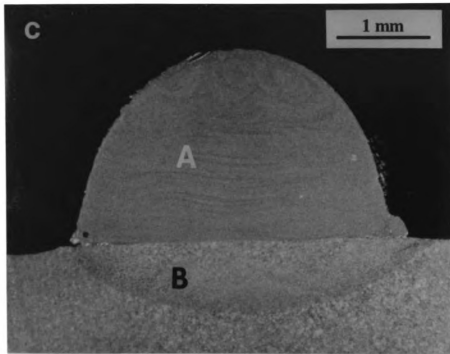


Figure 29- Three basic single clad bead profiles. (a) Deep penetration clad bead.  
(b) Clad bead with a reasonable width to height aspect ratio.  
(c) Parabolic clad bead. (A: clad. B: heat-affected zone)

Figure 29 (con'd)



Because the cutting blades on the rotary cutting die is 1.5 mm high, only parabolic clad track can meet the height requirement for the sake of cost-effectiveness. Figure 30 is a set of optical micrographs of the cross section of single clad tracks. The process variables are as follows: laser power = 2073 watts, spot size = 1.8 mm, and powder feed

rate = 0.167 gm/sec, and traverse speed varies from 3 to 6.6 mm/sec. Typically, three zones in a good clad track are observed: clad zone, interface zone, and heat-affected zone. The clad zone is the solidified molten alloy. The interface is a transitional zone between the clad zone and the substrate. The heat-affected zone is produced by the laser energy transferred to the substrate. The clad tracks look smooth, are free of porosity and macrocracks, and have complete fusion with the substrate but with minimum dilution.

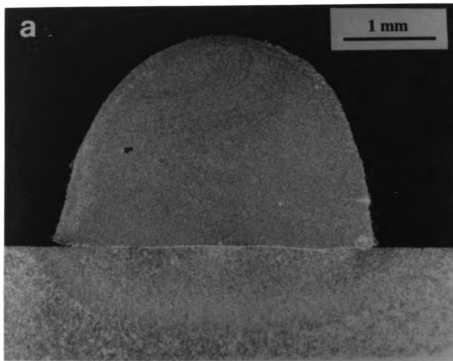


Figure 30- Optical micrographs of cross section of clad tracks with no macroscopic cladding defects. (a)  $v = 3$  mm/sec. (b)  $v = 3.9$  mm/sec. (c)  $v = 4.9$  mm/sec. (d)  $v = 5.8$  mm/sec. (e)  $v = 6.6$  mm/sec. Other processing parameters are as follows:  $P = 2073$  watts,  $D = 1.8$  mm, and  $F_p = 0.167$  gm/sec.



Figure 30 (con'd)

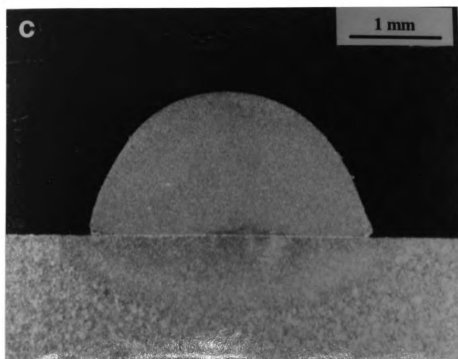
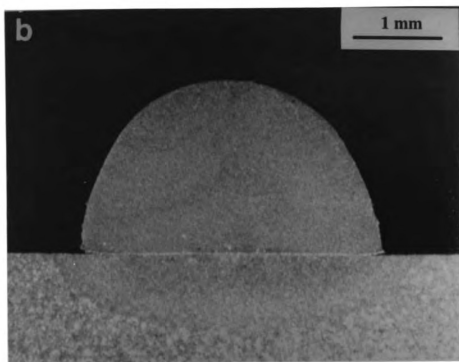


Figure 30 (con'd)

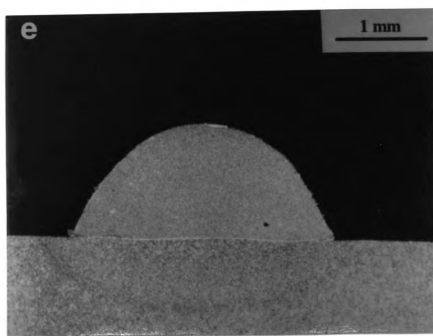
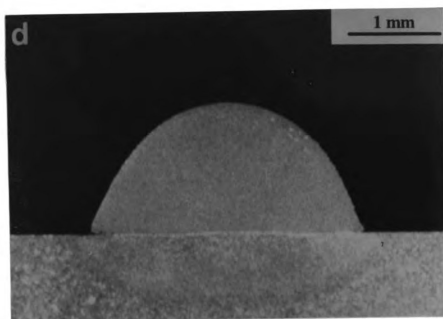


Figure 31 is another set of optical micrographs of cross section of single clad tracks, and shows the effect of laser power on the clad formation. The corresponding process parameters: traverse speed = 8.4 mm/sec, spot size = 2.3 mm, and powder feed rate = 0.167 gm/sec, and laser power varies from 1110 to 2073 watts. As mentioned before, when laser power decreases to 1110 watts, lack of fusion between the clad and substrate is observed, as shown in Figure 31 (d). Figure 32 is a higher magnified optical micrograph corresponding to Figure 31 (d). It clearly shows the debonding between the clad and substrate because energy density is not high enough to melt the substrate. The corresponding energy density is called the threshold energy density in this particular cladding system.

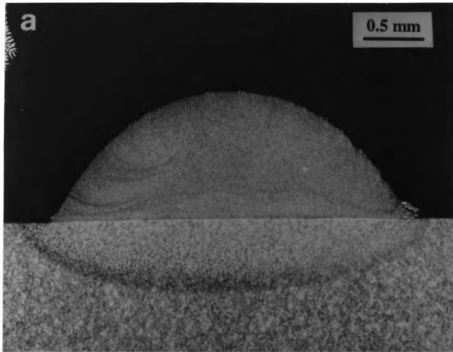


Figure 31- Effect of laser power on clad formation. (a)  $P = 2073$  watts. (b)  $P = 1755$  watts. (c)  $P = 1567$  watts. (d)  $P = 1110$  watts. Other processing parameters:  $v = 8.4$  mm/sec,  $D = 2.3$  mm, and  $F_p = 0.167$  gm/sec.

Figure 31 (con'd)

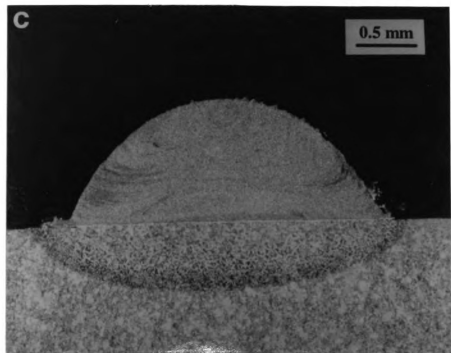
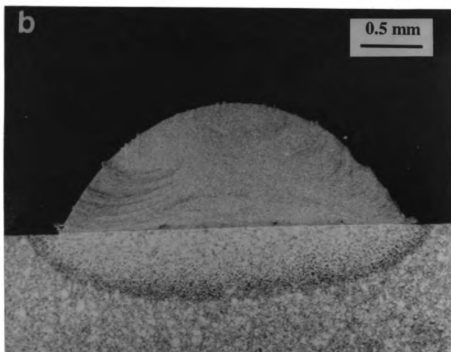


Figure 31 (con'd)

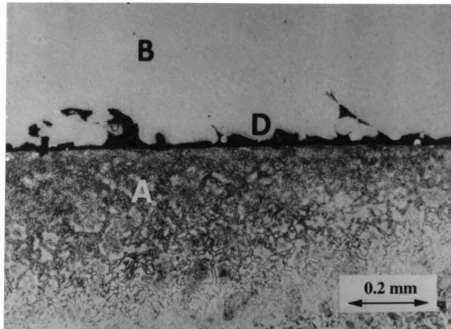
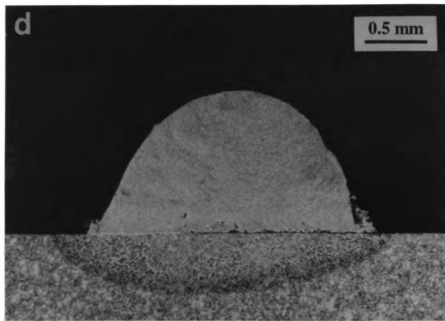
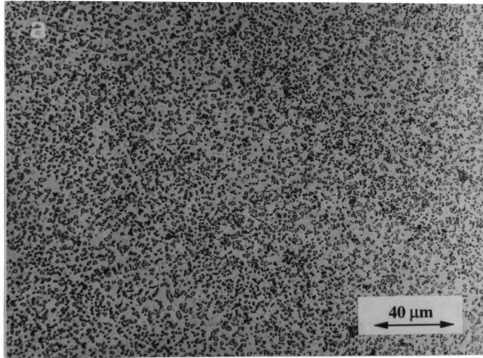


Figure 32- A magnified optical micrograph of figure 31 (d), showing the lack of fusion between the clad and the substrate (B: clad. A: HAZ. D: debonding).

### 5.9.2 Vanadium Carbides

Vanadium contents in CPM 10V and CPM 15V are up to about 10 and 15 wt. %, respectively. Its major influence is the formation of highly wear resistant carbides. Vanadium carbide is one of the hardest carbides found in high speed steels. These carbides also help maintain a very fine grain size at the high heat treating temperatures used for high speed steels because vanadium carbide is a thermodynamically stable intermetallic compound. Figure 33 (a) displays that fine vanadium carbide particles are uniformly dispersed in the matrix, which consists of martensite and retained austenite. Compared with the segregation and flake morphology of carbides in D2 alloy, as shown in Figure 33 (b), it is expected that wear resistant property of the cutting blades, which are made of CPM 15V by laser cladding process, will be significantly improved in the present process.



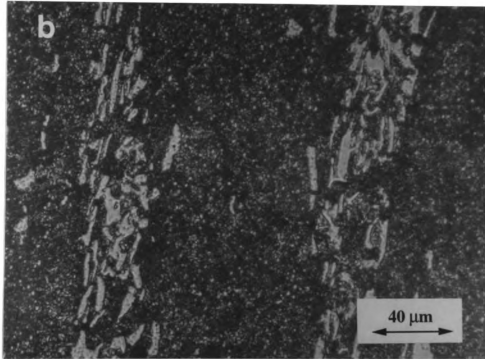


Figure 33- A view of carbides in CPM 10V and D2 alloys. (a) Fine vanadium carbide particles uniformly dispersed in the matrix in CPM 10V clad. (b) Segregation and flake morphology of carbides in D2 alloy.

### 5.10 Microhardness of A Single Clad Track

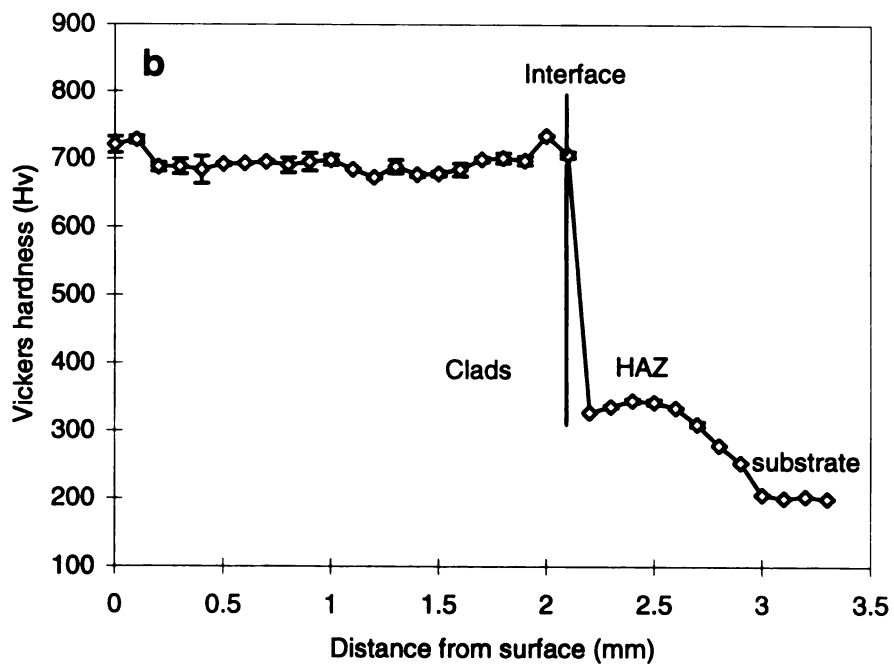
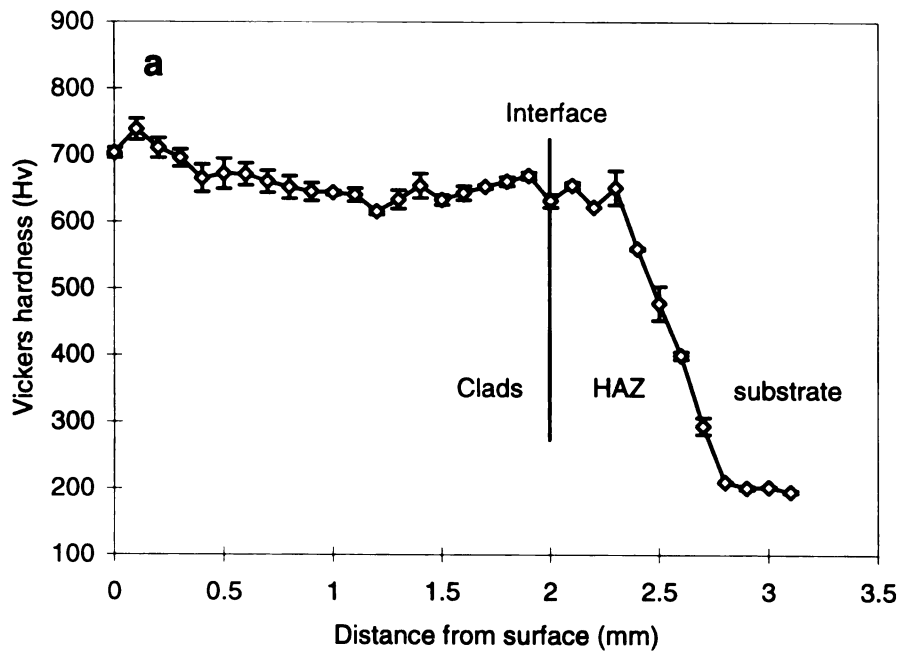
Figure 34 shows Vickers hardness measured from the CPM 10V clad to the substrate under different treatment conditions. The sample used to measure the hardness was made by the following processing parameters: laser power  $P = 2073$  watts,  $D = 2.3$  mm,  $v = 3$  mm/sec, and  $F_p = 0.167$  gm/sec.

The hardness of the as-clad sample is about 650 Hv, which is approximately equal to that of conventional tool steel D2 after standard heat treatment, as shown in Figure 34 (a).

Because retained austenite in high-alloy steels is extremely stable, it must be destabilized by tempering above 500 °C, and transformed to martensite. Also, the tempering treatment can further increase the hardness of the steel by secondary hardening and the formation of hard martensite [82-83]. For this reason, after the sample is double tempered at 540 °C for 15 minutes each, the hardness increases to about 700 Hv, as shown in Figure 34 (b).

After the tempered sample is dipped in liquid nitrogen for 15 minutes, the hardness increases to 850 Hv due to the transformation of the retained austenite to martensite, as shown in Figure 34 (c).





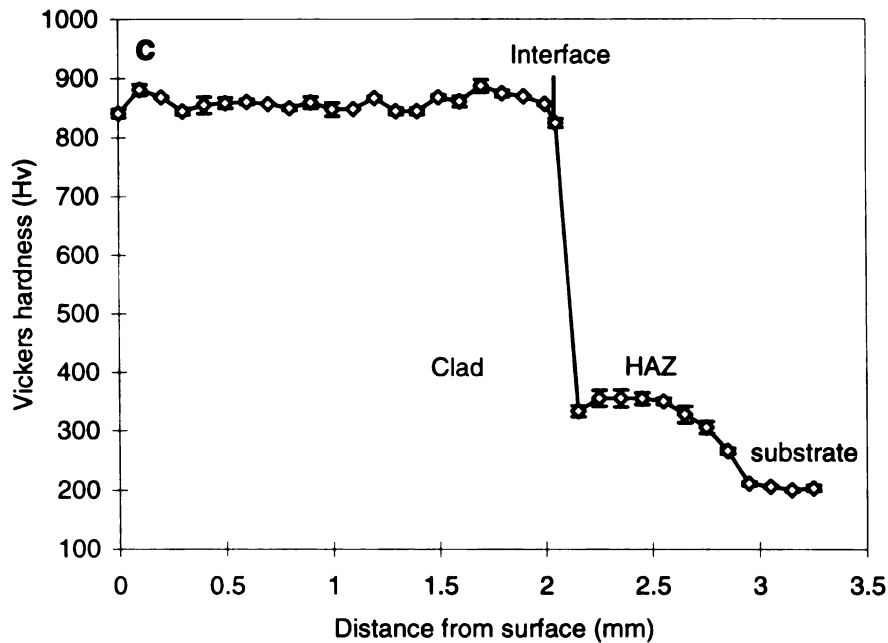


Figure 34- Microhardness profiles of the cladding track. (a) As-clad. (b) As-clad + tempering. (c) As-clad + tempering + liquid nitrogen treatment.

### 5.11 Manufacturing of Patterned Rotary Cutting Die

The other significant part of this research was aimed at depositing hard-facing tracks, with complicated geometric patterns, onto a AISI 1045 medium carbon steel roller to make rotary cutting die by laser cladding process. Based on the basic study, we investigated this feasibility in order to reach the final goal of this project.

Figure 35 shows a view of multiple hard-facing intersecting clad tracks on a flat plate. Cladding tracks are up to 1.5 mm thick, and 4.0 mm wide. They are smooth in appearance, metallurgically sound, and free of macrocracks in crossover region. The

process parameters used to produce this sample are given as follows: laser power = 2400 watts, spot size = 3.4 mm, traverse speed = 3.9 mm/sec, and powder feed rate = 0.167 gm/sec. Tool steel CPM 10V is used as the hard-facing material. This new process can be utilized to fabricate patterned flat plate cutting dies.

Finally, we tried to deposit hard-facing tracks, with complex geometric patterns, on a medium carbon steel roller by laser cladding process. The dimension of AISI 1045 steel roller is 305 mm (12") in length, and 101.6 mm (4") in diameter. Highly wear-resistant alloy CPM 15V is used as the clad material. CAD/CAM system is employed to fabricate a patterned rotary cutting die. The process variables are listed in Table 11.

Table 11- Processing parameters of producing rotary cutting dies

Samples	Material	Power P (watts)	Traverse speed v (mm/sec)	Spot size D (mm)	Powder feed rate F <sub>p</sub> (gm/sec)
A	CPM 15V	2370	4.7	2.3	0.25
B*	CPM 15V	2370	4.7	2.3	0.25

Samples	Energy density E <sub>d</sub> (J/mm <sup>2</sup> )	Cover gas flow rate (m <sup>3</sup> /hr)	Carrier gas flow rate (m <sup>3</sup> /hr)
A	279.2	1.27	0.62
B*	279.2	1.27	0.62

\* Sample B was preheated to 150 °C before laser cladding process.

Figure 36 is a view of the hard-facing tracks, directly deposited onto a AISI 1045 steel roller by laser cladding process. Figure 37 is another view of hard-facing tracks, with complex geometric patterns, deposited on a rotary cutting roller after laser cladding process (sample A). Hard-facing patterns with smooth surface are 1.8 mm high, and 3 mm wide, but macrocracks in crossover region were observed. With regard to the

macrocracks observed in Figure 37, the two reasons may be considered. The residual tensile stresses may result from high thermal gradients by laser cladding process and different thermal expansion behavior of the materials involved. When the residual thermal stresses exceed the fracture stress of the clad, cracks will be created. Material factor is intrinsic property of material itself, and can not be changed. The only factor which can be changed is the high thermal gradients, which lead to the reduction in thermal stresses. A simple but effective method is to preheat the workpiece to a certain temperature.

In this study, the AISI 1045 steel roller is preheated to 150 °C, and complex hard-facing patterns are deposited on it by laser cladding. Through examining the sample by using an **OLYMPUS PM-10AK** optical microscope just after laser cladding, no cracks in crossover region were observed. A fully functional prototype of an industrial cutting die, for pilot testing, has been successfully produced by this process (sample B), as shown in Figure 38. This new technique for manufacturing patterned rotary cutting dies is so successful that it is about to be implemented in cutting-die making industry.

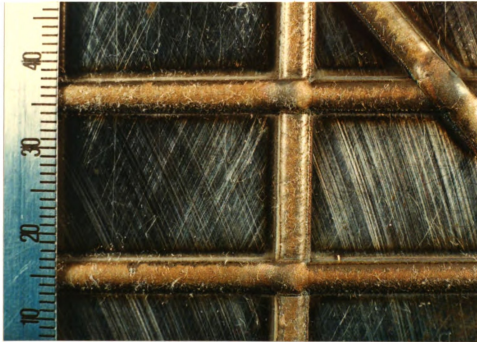


Figure 35- A view of intersecting hard-facing tracks, with smooth surfaces, uniform cladding thickness, and width, deposited on a AISI 1045 steel flat plate.

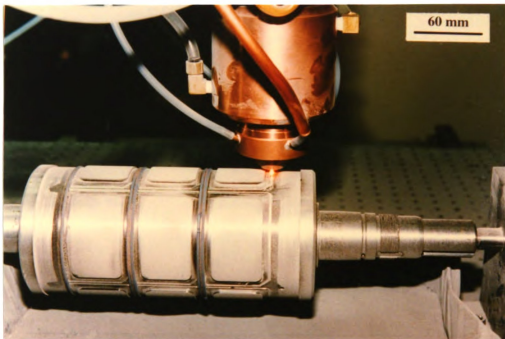


Figure 36- A view of the hard-facing tracks, directly deposited onto a AISI 1045 steel roller by laser cladding process.

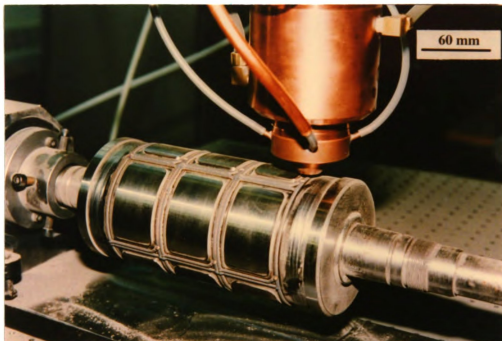


Figure 37- Hard-facing tracks, with complicated geometric patterns, deposited on a AISI 1045 steel roller via laser cladding (sample A).

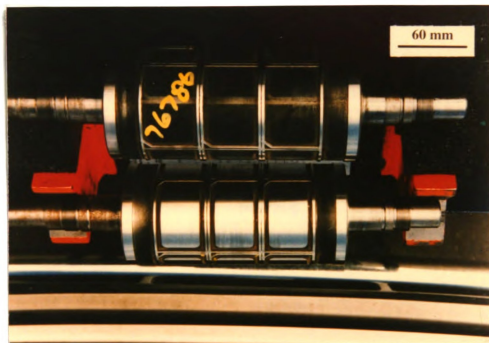


Figure 38- A view of hard-facing tracks, with complex geometric patterns, deposited on a steel roller by laser cladding after surface grinding (sample B).



## **Chapter 6**

### **CONCLUSIONS**

The following conclusions can be drawn from this research:

- The new powder delivery system designed for laser cladding avoids all the drawbacks of the lateral powder feeding systems. It can provide highly stable, continuous, and accurate powder feed rate, and deliver the powder stream coaxially into the molten pool with the laser beam to form high quality cladding tracks, with smooth surfaces, and uniform thickness and width. Also, this system is suited for deposition of complex geometric patterns on a flat plate or a curved surface for different applications, such as fabrication of rotary cutting dies, repair of turbine blades, and prototyping of forging dies. Most importantly, the new powder feeding system is suitable for on-line industrial production.
- For a given laser power and spot size, when the traverse speed varies from about 5 to about 10.5 mm/sec, and the powder feed rate varies from 0.1 to 0.25 gm/sec, powder utilization coefficient,  $\alpha$ , is constant for each process condition. This shows that value of  $\alpha$  is not related to traverse speed, and powder feed rate. However, it is related to spot size. When the laser-beam diameter "D" was 1.8 mm, the average value of  $\alpha$  was 0.71. For  $D \geq 2.3$  mm, average value of  $\alpha$  was 0.80.
- With other variables held constant, clad width modestly decreases as traverse speed increases. When traverse speed accelerates to 8.4 mm/sec, clad width is almost equal

to laser-beam diameter. This speed (for our particular system) is called the threshold traverse speed in this cladding system. Below the threshold traverse speed, the clad is much wider than spot size. Clad width gently increases with the increase of energy density when other parameters are kept constant. The clad gently widens as powder feed rate increases with other variables held constant.

- A simple but realistic model is developed, relating the maximum clad thickness and various process parameters. For a given alloy powder, if the powder feed rate and spot size are kept constant, the clad thickness is inversely proportional to traverse speed. While for fixed powder feed rate and traverse speed, the clad thickness is inversely proportional to the spot size. Finally, when traverse speed and spot size are held constant, the clad thickness is directly proportional to powder feed rate. In each case, the calculated results of this model are in good agreement with experimental results.
- A specific energy equation, suitable for a toroidal  $TEM_{01}$  beam mode, is developed. When laser power and traverse speed are kept constant, the energy density is inversely proportional to spot size. While laser power and spot size are held constant, the energy density is inversely proportional to traverse speed. If traverse speed and spot size are constant, the energy density is directly proportional to laser power.
- Thermal penetration depth is a function of energy density. For fixed traverse speed, spot size, and powder feed rate, the higher laser power, the higher is the energy density, and more energy is transferred to the substrate, and therefore the deeper is the heat-affected zone.
- Clad bead geometry is related to the processing parameters, such as power density, traverse speed, and powder feed rate. The deep penetration bead is produced at higher

power density or lower powder feed rate. The clad bead with a reasonable width to height aspect ratio is achieved using a correct balance of power density, traverse speed, and powder feed rate. The parabolic shape cross section, clad bead with a minimum dilution is produced at a higher powder feed rate and/or a lower traverse speed.

- Optical micrograph displayed that fine vanadium carbide particles are uniformly dispersed in the matrix. Compared with the segregation and flake morphology of carbides in D2 alloy, it is expected that wear-resistant property of the cutting blades (produced by laser cladding) will be significantly improved in the present process.
- A hardness of the cladding tracks up to 650 Hv has been achieved, and the hardness increases to 850 Hv after cooling to the liquid nitrogen temperature, which causes transformation of the retained austenite to martensite.
- A novel process for manufacturing plate or rotary cutting dies, with complicated geometric patterned cutting blades, has been successfully developed by directly laser surface cladding. Fully functional prototype of an industrial rotary cutting die, for pilot testing, has been successfully produced via laser cladding process. This new technique is being implemented in die-making industry.

## BIBLIOGRAPHY

- [1] J. Bartos, "The microstructure and abrasive wear test of different composite layers formed by laser coating," in *Laser Materials Processing: Industrial and Microelectronics Applications* (E. Beyer, M. Cantello, A. V. La Rocca, L. D. Laude, F. O. Olsen and G. Sepold, Eds.), SPIE vol. 2207, pp. 553-563, SPIE-The International Society for Optical Engineering, 1994.
- [2] W. Konig and P. K. Kirner, "Laser surface treatment prolongs tool life," in *Laser Materials Processing: Industrial and Microelectronics Applications* (E. Beyer, M. Cantello, A. V. La Rocca, L. D. Laude, F. O. Olsen and G. Sepold, Eds.), SPIE vol. 2207, pp. 44-52, SPIE-The International Society for Optical Engineering, 1994.
- [3] Leon-Fong, "The physics of lasers," in *Applied Laser Tooling* (O. D. D. Soares and M. Perez-Amore, Eds.), pp. 43-53, Martinus Nijhoff Publishers, 1987.
- [4] J. F. Ready, *Industrial Applications of Lasers*. New York: Academic Press, 1978
- [5] J. T. Verdeyen, *Laser Electronics*. Prentice-Hall, Inc., 1989.
- [6] D. C. Winburn, *Lasers*. Marcel Dekker, Inc., 1987.
- [7] B. A. Lengyel, *Introduction to Laser Physics*. John Wiley and Sons, Inc., 1967.
- [8] W. W. Duley, *CO<sub>2</sub> lasers - Effects and Applications*. New York: Academic Press, 1976.
- [9] W. M. Steen, *Laser Material Processing*. Springer-Verlag London Limited, 1991.
- [10] R. C. Crafer and P. J. Oakley, "Process and physical aspects of continuous wave laser processing," in *Applied Laser Tooling* (O. D. D. Soares and M. Perez-Amore, Eds.), pp. 55-79, Martinus Nijhoff Publishers, 1987.
- [11] Y. Arata and I. Miyamoto, "Some fundamental properties of high power laser beam as a heat source," in *Plasma, Electron & Laser Beam Technology* (Y. Arata, Ed.), pp.233-262, ASM, Metals Park, OH, 1986.

- [12] E. M. Breinan and B. H. Kear, "Rapid solidification laser processing at high power density," in *Laser Materials Processing* (M. Bass, Ed.), pp. 237-294, North-Holland Publishing Company, 1983.
- [13] T. Bell, "Surface heat treatment of steel to combat wear," *Acta Metallurgia*, vol. 49, no. 3, pp. 103-111, 1982.
- [14] J. Mazumder, "Laser heat treatment: the state of the art," *Journal of Metals*, vol. 35, no. 5, pp. 18-26, 1983.
- [15] V. G. Gregson, "Laser heat treatment," in *Laser Materials Processing* (M. Bass, Ed.), Ch. 4, North-Holland Publishing Company, 1984.
- [16] M. F. Ashby, and K. E. Easterling, "The transformation hardening of steel surfaces by laser beam," *Acta Metallurgia*, vol. 32, no. 11, pp. 1935-1948, 1984.
- [17] M. Tayal and K. Mukherjee, "Thermal and microstructural analysis for laser surface hardening of steel," *Journal of Applied Physics*, vol. 75, no. 8, pp. 3855-3861, 1994.
- [18] D. N. H. Trafford, T. Bell, J. H. P. C. Megaw, and A. D. Bransden, "Laser treatment of gray iron," *Metal Technology*, vol. 10, no. 2, pp. 69-77, 1983.
- [19] I. C. Hawkes, A. M. Walker, W. M. Steen, and D. R. F. West, "Application of laser surface melting and alloying to alloys based on the Fe-C system," in *Laser Processing of Materials* (K. Mukherjee and J. Mazumder, Eds.), pp. 169-182 AIME, Warrendale, PA, 1985.
- [20] H. W. Bergmann, "Laser surface melting of iron-base alloys," in *Laser Surface Treatment of Metals* (C. W. Draper and P. Mazzoldi, Eds.), pp. 351-368, Martinus Nijhoff Publishers, Dordrecht, Netherlands, 1986.
- [21] W. M. Steen, Z. D. Chen, and D. R. F. West, "Laser surface melting of cast irons and alloy cast irons," in *Industrial Laser Annual Hand book 1987* (D. Belforte and M. Levitt, Eds.), pp. 80-96.
- [22] W. J. Tomlinson and M. G. Talks, "Cavitation erosion of heat-treated low alloy cast irons," *Wear*, vol. 137, no. 1, pp. 143-146, 1990.
- [23] M. Gremaud, M. Carrard, and W. Kurz, "Microstructure of rapidly solidified Al-Fe alloys subjected to laser surface treatment," *Acta Metallurgica et Materialia*, vol. 38, no. 12, pp. 2587-2599, 1990.
- [24] M. Pierantoni and E. Blank, "Effect of laser surface remelting and alloying on the wear behaviour of Al-Si alloys," *Key Engineering Materials*, vol. 46-47, pp. 354-367, 1990.

- [25] J. M. Pelletier, D. Pergue, F. Fouquet, and H. Mazille, "Laser surface melting of low and medium carbon steels. Influence on mechanical and electrochemical properties," *Journal of Materials Science*, vol. 24, no. 12, pp. 4343-4349, 1989.
- [26] D. R. K. Rao, B. Venkataraman, M. K. Asundi, and G. Sundararajan, "Effect of lasersurface melting on the erosion behaviour of a low alloy steel," *Surface & Coatings Technology*, vol. 58, no. 2, pp. 85-92, 1993.
- [27] S. Saendig and P. Wiesner, "Laser surface melting of cutting tool materials," in *Laser Materials Processing* (P. Denney, I. Miyamoto, and B. L. Mordike, Eds.), vol. 2306, pp. 835-846. Publ. by Laser Inst. of America, Orlando, FL, USA, 1994.
- [28] R. Vilar, R. Colaco, and A. Almeida, "Laser surface treatment of tool steels," *Optical and Quantum Electronics*, vol. 27, no. 12, pp. 1273-1289, 1995.
- [29] C. Marsden, D. R. F. West and W. M. Steen, "Laser Surface Alloying of Stainless Steel with Carbon," in *Laser Surface Treatment of Metals* (C.W. Draper and P. Mazzoldi, Eds.), pp. 461-474. Martinus Nijhoff Publishers, Dordrecht, Netherlands, 1986.
- [30] T. Chande, A. Ghose, and J. Mazumder, "surface properties and microstructures of AISI 1016 steel laser surface alloyed with chromium and nickle," in *Laser Processing of Materials* (K. Mukherjee and J. Mazumder, Eds.), pp. 117-130. AIME, Warrendale, PA, 1985.
- [31] N. B. Dahotre, and K. Mukherjee, "Development of microstructure in laser surface alloying of steel with chromium," *Journal of Materials Science*, vol. 25, no.1B, pp. 445-454, 1990.
- [32] T. R. Tucker, A. H. Clauer, S. L. Ream and C. T. Walkers, "Rapidly solidified microstructures in surface layers of laser alloyed molybdenum on Fe-C substrates" in *Proc. Conf. Rapidly Solidified Amorphous and Crystalline Alloys* (B. H. Kear, B. C. Giessen, and M. Cohen, Eds.), pp 541-545. Elsevier Science Publ. Co. Inc., New York, USA, 1982.
- [33] C. W. Draper, "Laser surface alloying: the state of the art," in *Lasers in Metallurgy* (K. Mukherjee and J. Mazumder, Eds.), pp. 67-92. AIME, Warrendale, PA, 1981.
- [34] J. Mazumder, "Wear Properties of Laser Alloyed and clad Fe-Cr-Mn-C Alloys," in *Proc. ICALEO '84* (J. Mazumder, Ed.), vol. 44, pp. 159-167. Publ. by LIA, USA, 1985.
- [35] E. MaCattery and P. G. Moore, "Electrochemical behavior of laser-processed metal surface," in *Laser Surface Treatment of Metals* (C.W. Draper and P. Mazzoldi, Eds.), pp. 263-295. Martinus Nijhoff Publishers, Dordrecht, Netherlands, 1986.

- [36] L. Renaud, F. Fouquet, J. P. Millet, and J. L. Crolet, "Corrosion resistance of Fe-Ni-Cr laser surface alloys," *Surface & Coatings Technology*, vol. 45, no. 1-3, pp. 449-456, 1991.
- [37] M. A. Anjos, R. Vilar, R. Li, M. G. Ferreira, W. M. Steen, and K. Watkins, "Fe-Cr-Ni-Mo-C alloys produced by laser surface alloying," *Surface & Coatings Technology*, vol. 70, no. 2-3, pp. 235-242, January 1995.
- [38] E. Gaffet, J. M. Pelletier, and S. Bonnet-Jobez, "Laser surface alloying of Ni film on Al-based alloy," *Acta Metallurgica*, vol. 37, no. 12, pp. 3205-3215, 1989.
- [39] A. Almeida, R. Vilar, and R. Colaco, "Laser alloying of Al and 7175 Al alloy for enhanced corrosion resistance," in *Laser Materials Processing* (P. Denney, I. Miyamoto, and B. L. Mordike, Eds.), vol. 2306, pp. 903-912. Publ. by Laser Inst. of America, Orlando, FL, USA, 1994.
- [40] S. Yerramareddy and S. Bahadur, "Effect of laser surface treatments on the tribological behavior of Ti-6Al-4V," *Wear*, vol. 157, no. 2, pp. 245-262, 1992.
- [41] O. V. Akgun and O. T. Inal, "Laser surface modification of Ti-6Al-4V alloy," *Journal of Materials Science*, vol. 29, no. 5, pp. 1159-1168, 1994.
- [42] J. D. Ayers, "Particulate composite surfaces by laser processing," in *Lasers in Metallurgy* (K. Mukherjee and J. Mazumder, Eds.), pp. 115-125. AIME, Warrendale, PA, 1981.
- [43] J. D. Ayers and T. R. Tucker, "Particulate TiC hardened surface by laser melt injection," *Thin Solid Films*, vol. 73, pp. 201-207, 1980.
- [44] S. Ariely, J. Shen, M. Bamberger, F. Dausiger, and H. Hugel, "Laser surface alloying of steel with TiC," *Surface & Coatings Technology*, vol. 45, no.1-3, pp. 403-408, 1991.
- [45] B. Gruenenwald, E. Bischoff, J. Shen, and F. Dausinger, "Laser surface alloying of case hardening steel with tungsten carbide and carbon" *Materials Science and Technology*, vol. 8, no. 7, pp. 637-643, 1992.
- [46] D. Pantelis, H. Michaud, and M. de Freitas, "Wear behaviour of laser surface hardfaced steels with tungsten carbide powder injection," *Surface & Coatings Technology*, vol. 57, no. 2-3, pp. 123-131, 1993.
- [47] B. S. Yilbas, R. Davies, and Z. Yilbas, "Laser alloying of metal surfaces by injecting titanium carbide powders," *International Journal of Machine Tool & Manufacture*, vol. 29, no. 4, pp. 499-503, 1989.

- [48] X. B. Zhou and J.Th. M. De Hosson, "Metal-ceramic interfaces in laser coated aluminum alloys," *Acta Metallurgica et Materialia*, vol. 42, no. 4, pp.1155-1162, 1994.
- [49] J. H. Abboud and D. F. R. West, "Ceramic-metal composites produced by laser surface treatment," *Materials Science and Technology*, vol. 5, pp. 725-728, 1989.
- [50] J. A. Folkes and K. Shibata, "Laser cladding of Ti-6Al-4V with various carbide powders," *Journal of Laser Applications*, vol. 6, no. 2, pp. 88-94, 1994.
- [51] A. Weisheit and B. L. Mordike, "Laser surface alloying of titanium with VC and MoSi<sub>2</sub> to improve wear resistance," in *Laser Materials Processing* (P. Denney, I. Miyamoto, and B. L. Mordike, Eds.), vol. 2306, pp. 923-933. Publ. by Laser Inst. of America, Orlando, FL, USA, 1994.
- [52] K. Komvopoulos, "Effect of process parameters on the microstructure, geometry and microhardness of laser-clad coating materials," *Materials Science Forum*, vol. 163, no. 6, pt. 1, pp. 417-422, 1994.
- [53] K. P. Cooper and P. Slebodnick, "Recent development in lasser melt/particles injection processing," in *Laser Materials Processing* (G. Bruck, Ed.), pp. 3-16. Springer-Verlag: IFS (Publications) Ltd., UK, 1989.
- [54] J. Choi and J. Mazumder, "Non-equilibrium synthesis of Fe-Cr-C-W alloy by laser cladding," *Journal of Materials Science*, vol. 29, no. 17, pp. 4460-4476, 1994.
- [55] A. Frenk and W. Kurz, "High speed laser cladding: solidification conditions and micostructure of a cobalt-based alloy," *Materials Science ane engineering*, vol. A173, pp. 339-342, 1993.
- [56] W. Alhua, T. Zengyi, and Z. Beidi, "Laser beam cladding of srating surfaces on exhaust valves," *Welding Research Supplement*, vol. 70, no. 4, pp. 106s-109s, 1991.
- [57] S. J. Matthews, "Laser fusing of hardfacing alloy powders," in *Laser in Materials Processing* (E. A. Metzbower, Ed.), pp. 138-148. ASM, Metals Park, OH, 1983.
- [58] B. C. Oberlander and E. Lugscheider, "Composition of properties of coatings produced by laser cladding and conventional methods," *Materials Science and Technology*, vol. 8, pp. 657-665, August 1992.
- [59] T. Takeda, W. M. Steen, and D. R. F. West, "Laser Cladding with Mixed Powder Feed", in *Proc. conf. ICALEO '84* (J. Mazumder, Ed.), vol. 44, pp. 151-158, Publ. by LIA, 1985.



- [60] P. Sallamand and J. M. Pelletier, "Laser cladding on aluminium-base alloys: Microstructural features," *Materials Science and Engineering*, vol. A171, no. 1-2, pp. 263-270, 1993.
- [61] Y. Liu, J. Koch, J. Mazumder, and K. Shibata, "Processing, microstructure, and properties of laser-clad Ni alloy FP-5 on Al alloy AA333," *Metallurgical Transactions*, vol. 25B, pp. 425-434, 1994.
- [62] C. Ribaudo, S. Sircar, and J. Mazumder, "Laser-clad  $\text{Ni}_{70}\text{Al}_{20}\text{Cr}_7\text{Hf}_3$  alloys with extended solid solution of Hf. Part II: Oxidation behavior," *Metallurgical Transactions*, vol. 20A, no. 11, pp. 2267-2277, 1989.
- [63] J. De Damborenea and A. J. Vazquez, "Laser cladding of high-temperature coatings," *Journal of Materials Science*, vol. 28, pp. 4775-4780, 1993.
- [64] G. Abbas and D. R. F. West, "Laser surface cladding of stellite and stellite-SiC composite deposits for enhanced hardness and wear," *Wear*, vol. 143, no. 2, pp. 353-363, 1991.
- [65] Y. P. Pei, J. H. Ouyang, T. C. Lei, and Y. Zhou, "Microstructure of laser-clad SiC-(Ni alloy) composite coating," *Materials Science & Engineering*, vol. A194, no. 2, pp. 219-224, 1995.
- [66] H. W Gu, "Laser cladding of Ni based WC alloy," *Jiguang Jishu/Laser Technology*, vol. 17, no. 4, pp.220-223, 1993.
- [67] E. Ramous, L. Giordano, A. Tiziani, B. Badan, and M. T. Cantello, "Laser cladding of ceramic and metallic coatings on steel," *Key Engineering Materials*, vol. 46-47, pp. 425-433, 1990.
- [68] W. Cerri, R. Maryinella, and G. P. Mor, "Laser deposition of carbide-reinforced coatings," *surface and Coatings Technology*, vol.49, pp. 40-45, 1991.
- [69] A. Techel, A. Luft, A. Mueller, and S. Nowotny, "Production of hard metal-like protection coatings by  $\text{CO}_2$  laser cladding," *Optical and Quantum electronics*, vol. 27, no. 12, pp. 1313-1318, 1995.
- [70] D. S. Gnanamuthu, "Laser surface treatment," in *Source Book on Applications of the Laser in Metalworking*, pp. 324-358, ASM, Metals Park, OH, 1981.
- [71] J. I. Nurminen and J. E. Smith, "Parametric evaluation of laser/clad interaction for hardfacing applications," in *Lasers in Materials Processing* (E. A. Metzbower, Ed.), pp. 94-106, ASM, Metals Park, OH, 1984.

- [72] E. M. Breinan, D. B. Snow, C. O. Brown, and B. H. Kear, "New developments in laser melting using continuous prealloyed powder feed," in *Source Book on Applications of the Laser in Metalworking*, pp. 279-291, ASM, Metals Park, OH, 1981.
- [73] V. M. Weerasinghe and W. M. Steen, "Laser Cladding with Pneumatic Powder Delivery," In *Lasers in Materials Processing* (E. A. Metzbower, Ed.), pp. 166-175, ASM, Metals Park, OH, 1984.
- [74] R. P. Harrison, "Laser powder welding," *Turbomachinery International*, vol. 35, no. 6, pp. 52-53, 1994.
- [75] P. A. Vetter, Th. Engel, and J. Fontaine, "Laser cladding: the relevant parameters for process control," in *Laser Materials Processing: Industrial and Microelectronics Applications* (E. Beyer, M. Cantello, A. V. La Rocca, L. D. Laude, F. O. Olsen and G. Sepold, Eds.), SPIE vol. 2207, pp. 452-462, SPIE-The International Society for Optical Engineering, 1994.
- [76] W. M. Steen, "Laser surface cladding," in *Laser Surface Treatment of Metals* (C.W. Draper and P. Mazzoldi, Eds.), pp. 369-387, Martinus Nijhoff Publishers, Dordrecht, Netherlands, 1986.
- [77] O. D. D. Soares, "Applied laser tooling," in *Applied Laser Tooling* (O. D. D. Soares and M. Perez-Amore, Eds.), pp. 1-24, Martinus Nijhoff Publishers, 1987.
- [78] R. M. Macintyre, "The use of lasers in Rolls-Royce," in *Laser Surface Treatment of Metals* (C.W. Draper and P. Mazzoldi, Eds.), pp. 545-549, Martinus Nijhoff Publishers, Dordrecht, Netherlands, 1986.
- [79] Minoru Kawasaki, Koyu Takase, Sinji Kato, Masahiro Nakagawa, and Kazuhiko Mori, "Development of engine valve seats directly deposited onto aluminum cylinder head by laser cladding process," In *SAE Technical Paper Series*, pp.1-15, Publ. by SAE, Warrendale, PA, 1992. SAE Paper No. 920571.
- [80] K. E. Pinnow and W. Stasko, "P/M tool steels," in *Metals Handbook*, vol. 1, 10th Ed. pp. 780-792, ASM, Metals Park, 1990.
- [81] A. Belmondo and M. Castagna, "Wear-resistant coatings by laser processing," in *Source Book on Applications of the Laser in Metalworking*, pp. 310-317, ASM, Metals Park, OH, 1981.
- [82] R. Colaco and R. Vilar, "Laser surface melting of bearing steels," in *Laser Applications for Mechanical Industry* (S. Martellucci, and A. Scheggi, Eds.), pp. 305-314, Kluwer Academic Publishers, 1992.

- [83] Q. F. Peng, Z. Shi, and I. M. Hancock, and A. Bloyce, "Energy beam surface treatment of tool steels and their wear," *Key Engineering Materials*, vol. 46-47, pp. 229-244, 1990.

MICHIGAN STATE UNIV. LIBRARIES



31293015592771